JNeurosci
THE JOURNAL OF NEUROSCIENCE

Research Articles: Behavioral/Cognitive

Temporal dynamics and response modulation across the human visual system in a spatial attention task: an ECoG study

Anne B. Martin[1,9], Xiaofang Yang[2], Yuri B. Saalmann[1,10], Liang Wang[1,11], Avgusta Shestyuk[3], Jack J. Lin[5,6,7], Josef Parvizi[8], Robert T. Knight[3,4] and Sabine Kastner[1,2]

[1]*Princeton Neuroscience Institute*
[2]*Department of Psychology, Princeton University*
[3]*Helen Wills Neuroscience Institute*
[4]*Department of Psychology, University of California, Berkeley*
[5]*Center for the Neurobiology of Learning and Memory*
[6]*Department of Biomedical Engineering,*
[7]*Department of Neurology, University of California, Irvine*
[8]*Department of Neurology and Neurological Sciences, Stanford University*
[9]*Division of Biology and Biological Engineering, California Institute of Technology*
[10]*Department of Psychology, University of Wisconsin-Madison*
[11]*CAS Key Laboratory of Mental Health, Institute of Psychology, Chinese Academy of Sciences*

https://doi.org/10.1523/JNEUROSCI.1889-18.2018

Received: 23 July 2018

Revised: 15 October 2018

Accepted: 6 November 2018

Published: 20 November 2018

Author contributions: A.B.M., X.Y., and L.W. analyzed data; A.B.M., X.Y., Y.B.S., L.W., A.S., J.J.L., J.P., R.K., and S.K. edited the paper; A.B.M., X.Y., and S.K. wrote the paper; Y.B.S. and S.K. designed research; A.S., J.J.L., J.P., and R.K. performed research.

Conflict of Interest: The authors declare no competing financial interests.

We thank Michael Arcaro for help with implementing the probabilistic atlas. This work was supported by the National Institute of Mental Health Conte Center grant 1P50MH109429 (S.K., R.K. & J.P.), the National Institute of Mental Health grants R01MH064043 (S.K. & R.K.), R01MH109954 (J.P.) and R01MH110311 (Y.B.S.), the National Institute of Neurological Disorders and Stroke grant R01R37NS21135 (R.K.), and the James S. McDonnell Foundation 21st Century Science Initiative — Understanding Human Cognition — collaborative grant (S.K. & R.K.).

Correspondence should be addressed to Dr. Sabine Kastner, Princeton Neuroscience Institute and Department of Psychology, Washington Road, Princeton, NJ 08544. E-mail: skastner@princeton.edu

Cite as: J. Neurosci 2018; 10.1523/JNEUROSCI.1889-18.2018

Temporal dynamics and response modulation across the human visual system in a spatial attention task: an ECoG study

Abbreviated title: Electrocorticography of visual attention

Anne B. Martin[1,9], Xiaofang Yang[2], Yuri B. Saalmann[1,10], Liang Wang[1,11], Avgusta Shestyuk[3], Jack J. Lin[5,6,7], Josef Parvizi[8], Robert T. Knight[3,4] and Sabine Kastner[1,2]*

[1]Princeton Neuroscience Institute and [2]Department of Psychology, Princeton University; [3]Helen Wills Neuroscience Institute and [4]Department of Psychology, University of California, Berkeley; [5]Center for the Neurobiology of Learning and Memory, [6]Department of Biomedical Engineering, and [7]Department of Neurology, University of California, Irvine; [8]Department of Neurology and Neurological Sciences, Stanford University; [9]Division of Biology and Biological Engineering, California Institute of Technology; [10]Department of Psychology, University of Wisconsin-Madison; [11]CAS Key Laboratory of Mental Health, Institute of Psychology, Chinese Academy of Sciences

*Correspondence should be addressed to Dr. Sabine Kastner, Princeton Neuroscience Institute and Department of Psychology, Washington Road, Princeton, NJ 08544. E-mail: skastner@princeton.edu.

Conflict of interest: The authors declare no competing financial interests.

Keywords: Spatial Response Fields, Onset Latencies, Attention Latencies, Topographic Atlas

Manuscript information: 11 figures and 5 tables; 74 pages.

Abstract 244 words

Significance statement 120 words

Introduction 540 words

Discussion 1860 words

Acknowledgements: We thank Michael Arcaro for help with implementing the probabilistic atlas. This work was supported by the National Institute of Mental Health Conte Center grant 1P50MH109429 (S.K., R.K. & J.P.), the National Institute of Mental Health grants R01MH064043 (S.K. & R.K.), R01MH109954 (J.P.) and R01MH110311 (Y.B.S.), the National Institute of Neurological Disorders and Stroke grant R01R37NS21135 (R.K.), and the James S. McDonnell Foundation 21st Century Science Initiative – Understanding Human Cognition – collaborative grant (S.K. & R.K.).

ABSTRACT

The selection of behaviorally relevant information from cluttered visual scenes (often referred to as 'attention') is mediated by a cortical large-scale network consisting of areas in occipital, temporal, parietal, and frontal cortex that is organized into a functional hierarchy of feedforward and feedback pathways. In the human brain, little is known about the temporal dynamics of attentional processing from studies at the mesoscopic level of electrocorticography (ECoG), that combines millisecond temporal resolution with precise anatomical localization of recording sites. We analyzed high frequency broadband responses (HFB) responses from 626 electrodes implanted in 8 epilepsy patients, who performed a spatial attention task. Electrode locations were reconstructed using a probabilistic atlas of the human visual system. HFB responses showed high spatial selectivity and tuning, constituting ECoG response fields (RFs), within and outside the topographic visual system. In accordance with monkey physiology studies, both RF widths and onset latencies increased systematically across the visual processing hierarchy. We utilized the spatial specificity of HFB responses to quantitatively study spatial attention effects and their temporal dynamics to probe a hierarchical top-down model suggesting that feedback signals back propagate the visual processing hierarchy. Consistent with such a model, the strengths of attentional modulation were found to be greater and modulation latencies to be shorter in posterior parietal cortex, middle temporal cortex and ventral extrastriate cortex as compared to early visual cortex. However, inconsistent with such a model, attention effects were weaker and more delayed in anterior parietal and frontal cortex.

SIGNIFICANCE STATEMENT

In the human brain, visual attention has been predominantly studied using methods with high spatial, but poor temporal resolution such as fMRI, or high temporal, but poor spatial resolution such as EEG/MEG. Here, we investigate temporal dynamics and attention effects across the human visual system at a mesoscopic level that combines precise spatial and temporal measurements by using electrocorticography in epilepsy patients performing a classical spatial attention task. Electrode locations were reconstructed using a probabilistic atlas of the human visual system, thereby relating them to topography and processing hierarchy. We demonstrate regional differences in temporal dynamics across the attention network. Our findings do not fully support a top-down model that promotes influences on visual cortex by reversing the processing hierarchy.

INTRODUCTION

The selection of information from cluttered visual environments (often referred to as 'attention') is a fundamental problem in cognitive neuroscience. This process is mediated by a cortical large-scale network consisting of areas in occipital, temporal, parietal, and frontal cortex (Desimone and Duncan, 1995; Kastner and Ungerleider, 2000; Corbetta and Shulman, 2002; Saalmann and Kastner, 2011; Caspari et al., 2015; Buschman and Kastner, 2015; Moore and Zirnsak, 2017). Anatomical and functional studies indicate that this network is organized into a hierarchy of feedforward and feedback pathways that are dynamically modulated by attention for selective routing of information. Anatomically, this processing hierarchy is constrained by specific laminar projection patterns that index feedforward and feedback connectivity (Felleman and Van Essen, 1991; Markov et al., 2014). Functionally, it is characterized by inter-areal interactions that use distinct frequency channels indexing feedforward and feedback signaling (van Kerkoerle et al., 2014; Bastos et al., 2015; Michalareas et al., 2016). Evidence from studies in patients suffering from attentional deficits due to brain damage, as well as inactivation and microstimulation studies in non-human primates, indicate that fronto-parietal areas generate attention-related modulatory signals that are fed back to sensory cortex (Barceló et al., 2000; Moore and Armstrong 2003; Corbetta and Shulman 2011). Consistent with such a feedback model of attention control, it has been shown in monkey physiology studies that modulatory attention effects are greater and modulation latencies are shorter in higher-order as compared to lower-order cortex, suggesting that attention-related feedback signals reverse the visual processing hierarchy (Mehta et al., 2000; Buffalo et al., 2010).

In the human brain, selective attention has been predominantly studied with methods that emphasize network level analyses and have either relatively high spatial, but poor temporal resolution such as fMRI, or high temporal, but relatively poor spatial resolution such as MEG/EEG. The functional hierarchy of feedforward and feedback pathways based on inter-areal interactions has been recently reported for the human visual system using MEG (Michalareas et al., 2016). However, the precise temporal dynamics during feedforward and feedback selective visual processing are not known. Only few studies have been performed at the mesoscopic level of intracranial EEG, or electrocorticography (ECoG), that combines millisecond temporal resolution with precise anatomical localization of recording sites (for a review, see Parvizi and Kastner, 2018). In particular, high frequency broadband (HFB) responses above 70 Hz show time-locking to specific sensory, motor, and cognitive events (Kreiman et al., 2006; Flinker et al., 2011; Hermes et al., 2012; Mesgarani et al., 2014). Thus far, spatially and feature-specific attentional modulation of HFB responses have been reported in visual cortex (Yoshor et al., 2007; Davidesco et al., 2013; Szczepanski et al., 2014).

Here, we studied HFB responses from hundreds of electrodes covering occipital, temporal, parietal, and frontal cortex in patients performing a classical spatial attention task. Electrode locations were reconstructed using a probabilistic atlas of the human visual system (Wang et al., 2015), thereby relating them to topography and processing hierarchy. We characterized the spatial specificity of HFB responses and utilized this property to quantitatively study spatial attention effects on baseline and visually-evoked activity across topographic and non-topographic cortex. Further, we investigated

response onset and attentional modulation latencies to characterize the temporal dynamics of feedforward and feedback processing across the visual system during spatial attention.

MATERIALS AND METHODS

Subjects

Eight subjects (S1-S8, 6 males, age: 35 +/- 5, mean +/- SEM; see **Table 1** for further information), who underwent pre-surgical epilepsy evaluation, provided written informed consent to participate in the study. Experimental procedures were approved by the Institutional Review Boards of the participating institutions. Anti-epileptic medications were discontinued for 2-3 days before testing, and subjects were seizure free for at least five hours before testing. Subjects had normal or corrected-to-normal vision.

Subjects were implanted with 52-128 electrodes (1 cm spacing in grids and strips), covering extensive parts of frontal, parietal, occipital, and temporal cortex in their left (7 subjects) and right (1 subject) hemispheres (see **Figure 1** for electrode locations from all subjects and **Table 1** for coverage information of each subject). The positioning of electrode grids and strips was entirely based on clinical criteria pertaining to diagnostic procedures.

Visual display, stimuli, and task

Visual displays were generated on a Dell Precision M4600 laptop (Dell Inc.) using Presentation software (Neurobehavioral Systems, Inc.). Light gray stimuli were presented on a darker gray background at 50% contrast (**Figure 2A**). The timing of visual and auditory stimulus presentations was verified using a custom photodiode and microphone system. A microphone recorded auditory cues (starting tone and response feedback sounds; see below for task description). A photodiode placed at the lower right

corner of the monitor recorded timing of each visual stimulus using a simultaneous light square presented at the location of the photodiode receptor. The computer screen was placed at a distance of approximately 80 cm from the subject's eyes.

Subjects performed a variant of the Eriksen flanker task (Eriksen and Eriksen, 1974; Eriksen, 1995; Saalmann et al., 2012), discriminating between one of two target shapes that were shown embedded in a circular array of distracter shapes (**Figure 2A**). Subjects were instructed to maintain fixation throughout the duration of each trial. Following a 2 s inter-trial interval, each trial started with the presentation of a central fixation point (0.5°) and a coincidental tone. After 1100 ms, a circular spatial cue (1.5°) was displayed for 100 ms at a pseudo-randomly chosen peripheral location (7° eccentricity), followed by a variable delay period (300-700 ms) and the presentation of a circular array of equally spaced barrel and bowtie shapes (each approximately 2×2°). The array was displayed for 2000 ms or until the subject responded, indicating with a left or right mouse-button press, respectively, whether a barrel or bowtie shape was presented at the cued location. Barrel and bowtie target stimuli were presented randomly with equal likelihood, and flanking shapes were either congruent (same shape in nearest neighboring positions) or incongruent (different shape in nearest neighboring positions). Feedback on performance was given to the subject upon completion of each trial via tones signaling a correct or incorrect response. In order to minimize stress for the patients, they were instructed to emphasize accuracy rather than speed of responses. Following task instructions, subjects performed a training block to familiarize themselves with the task. During the experiment, trials were presented in blocks of 50,

and 3-6 blocks were recorded per subject (see **Table 1**). The number of cued locations and shapes in the target array was 8 (1 subject), 14 (5 subjects), or 16 (2 subjects).

To confirm fixation performance throughout the task, eye movements were visually monitored by the experimenter, and video recordings of the patient's face and eyes were performed throughout the experiment in the epilepsy monitoring care unit. No systematic saccadic eye movements were observed during task performance.

Data acquisition

Electrophysiological and peripheral (photodiode and microphone) channels were recorded using a 128-channel Tucker-Davis Technologies recording system at Stanford, a 128-channel Stellate Harmonic or Blackrock recording system at Johns Hopkins, a 128-channel Nihon Kohden recording system at Children's Hospital, and a 256-channel Nihon Kohden recording system (model JE120A) at UC Irvine. Signals were sampled at 3,052 Hz (Tucker-Davis), 1,000 Hz (Stellate), 5,000 Hz (Nihon Kohden) or 10,000 Hz (Blackrock), amplified and filtered (0.5-300 Hz at Stanford; 0.1-350 Hz (Stellate), or 0.3-2,500 Hz (Blackrock) at Johns Hopkins), using a subdural electrode reference and a scalp ground. Data were digitized and resampled offline at 1000 Hz to equate analysis across sites.

Electrode localization

For subjects S1-6, post-operative CT images of the implanted electrodes were aligned with pre-operative structural MRIs. For localization of electrodes within the visual

system, a probabilistic atlas of visuospatial topographic areas, which is based on fMRI retinotopic mapping data from 53 healthy subjects (Wang et al., 2015), was combined with each subject's structural MRI. Specifically, after obtaining co-registration parameters between the MRI and CT images using normalized mutual information algorithms implemented in Bioimage Suite software, electrode locations were mapped onto a rendering of the 3-D brain surface that was generated from the subject's structural MRI volume using FreeSurfer software (Dale et al., 1999; Fischl et al., 1999) and converted to a standard surface template using SUMA (Saad et al., 2004) and AFNI software. The probabilistic atlas of visuospatial topographic areas (Wang et al., 2015) was then superimposed onto each subject's brain surface. Using the maximum probability map, which assigns each node in the standard space to the topographic area with the highest probability, each electrode location that overlapped with the atlas was assigned to its maximally probable area. Sites that did not overlap the maximum probability map but were within one grid spacing (N = 17, 10 mm spacing) to the nearest maximally probable area were included with the area. For subjects S7 and S8, the electrode locations were reconstructed on a standard surface based on post-operative drawings of the electrode positions. The electrode grids in these two subjects did not overlap with the probabilistic atlas. Recording sites outside visuospatial topographic areas were located using the Harvard-Oxford cortical parcellation that is based on anatomical markers (Desikan et al., 2006).

Data analysis

Behavioral data. For each subject, accuracy (as the proportion of correct trials relative to the number of all trials) and mean reaction times (RTs; averaged across all correct trials) were computed. Trials with RTs > 3 standard deviations from the mean were excluded from analyses (median 2% of trials, min = 0.5%, max = 3.5%). We also computed accuracy as a function of flanker condition to determine behavioral flanker effects (i.e. higher accuracy for congruent than incongruent conditions). Since response speed was not emphasized in our task, RTs were not a reliable measure of flanker effects. For the analyses of neural data, only trials with correct responses and appropriate RTs were included; there were insufficient numbers of incorrect trials for reliable analysis.

Neural data – preprocessing and time frequency analysis. A neurologist manually inspected all ECoG channels to identify those with interictal or ictal epileptiform activity and artifacts. Channels and epochs contaminated by epileptiform activity or abnormal signals (e.g. poor contact, excess drift, high frequency noise) as well as those located over MRI defined abnormal sites were excluded from analysis (see **Table 1** for number of electrodes recorded and analyzed per subject). We excluded 16% of recorded electrodes based on these criteria (122/758). Offline, the intracranial field potentials (IFPs) from the remaining 636 electrodes recorded across the 8 subjects were referenced to each subject's common average. Power line noise and its harmonics were removed using a two-way zero phase-lag finite impulse response notch filter (±2 Hz).

All analyses were performed using the EEGLAB toolbox (Delorme and Makeig, 2004) and customized scripts written in Matlab (Mathworks, Inc.). Time series were aligned separately to the cue and array onset and sorted by cue location. To increase the number of trials available for each analysis, trials from each cue location were combined with the two closest locations on either side (only in cases of 14-16 cue locations). This resulted in spatial smoothing around each location of approximately 25 degrees of visual angle, yielding a minimum of 25 correct trials per cue location.

For each electrode, power spectra were calculated by applying a Hilbert transform to band pass filtered ECoG IFPs. First, the IFPs were filtered using a two-way zero phase-lag finite impulse response filter. We defined the filter order as 3r, where r is the ratio of the sampling rate to the low-frequency cutoff of the filter, rounded down, in each of the pass bands described below. For full spectrum analyses, we used multiple logarithmically-spaced pass bands with partially overlapping bands from 0.5-250 Hz *(*as in Voytek et al., 2013): the first pass band was seeded such that $f_{p(1)} = [0.5\ 0.9]$, and in subsequent bands $f_{L(n)} = 0.85 \times (f_{H(n-1)})$ and $f_{H(n)} = 1.1 \times (f_{H(n-1)} - f_{L(n-1)}) + f_{L(n)}$. We applied the Hilbert transform to each filtered time series *x* to acquire the analytic amplitude $a_x(n)$. The instantaneous power in band $f_{p(n)}$ at each time point in *x* is the mean over trials of $a_x(n)$. In this report, we focus our analyses on task-related power modulations in high-frequency broadband (HFB) responses above 70 Hz due to their high spatial specificity and temporal precision (Crone et al., 1998; Crone et al., 2006; Cheung et al., 2016; Parvizi and Kastner, 2018). While the neural basis of HFB responses is still not entirely clear, these signals have been shown to correlate with multi-unit activity

obtained from thousands of neurons in the immediate vicinity of the recording electrode (Ray et al., 2008a; Ray and Maunsell, 2011; Rich and Wallis, 2017; Watson et al., 2018). More recent findings indicate CA+ dendritic spikes in supragranular cortex as a principle contributor to pial HFB responses (Leszczyński et al., 2018). Here, HFB responses were defined as the average power between the pass bands centered at 70 and 200 Hz. These band definitions applied to the logarithmically-spaced bands yielded averages between 61.6-206.6 Hz.

Outlier time points (HFB power modulations greater than 6 standard deviations of the mean for time points in the 50-400 ms following cue and array onset), and trials with outlier cue- or array-evoked power compared to other trials of that same condition (each trial mean in the interval 50-300 ms following the cue or array greater than 6 standard deviations of the mean across all trials in that condition) were eliminated. Typically, fewer than 6% of trials per electrode were excluded (median 5%, min = 0%, max = 16%).

Identification of task-related activity. For each electrode, the mean IFP HFB power was calculated for each of the 8-16 peripheral locations and for four task-related epochs: cue-evoked (50-250 ms after cue onset), delay-related (200 ms before array onset), early array-evoked (50-200 ms after array onset), and late array-evoked (300-500 ms after array onset). HFB power fluctuations during these epochs were compared to baseline activity occurring 200 ms before cue onset. Because there is no sharp transition in the signals between cue-evoked and delay activity, we defined the length of

282 the presumed cue-evoked time interval post-hoc based on the time course of cue-
283 evoked activity in topographic area V1d/v, which showed a sharp decline of cue-evoked
284 responses after 250 ms and did not appear to show any elevated delay activity in our
285 recordings (e.g. **Figure 4A**, red trace). To avoid contamination of cue-evoked (i.e.
286 sensory-driven) with delay-related (i.e. driven by the cognitive state) activity, only trials
287 with delays longer than 450 ms (the median split of trials) were used for all analyses
288 regarding delay-related activity. Similarly, to avoid contamination from motor responses,
289 trials with reaction times shorter than 500 ms were excluded from analyses of array-
290 related activity (median 0, min = 0, max = 9).
291
292 Task-responsive recording sites were identified based on the following criteria. First, a
293 non-parametric cluster method (described below) was used to determine whether
294 significant cue-evoked HFB power (as compared to baseline) was sustained for at least
295 100 consecutive milliseconds at any of the peripheral locations. Second, the reliability of
296 the trial-wise power at those locations was measured by generating bootstrapped
297 distributions of the mean power during the cue-related epoch (1000 re-samplings over
298 trials of the cue-evoked HFB power relative to the mean baseline power); sites were
299 included only if the 95% confidence interval of the bootstrapped distribution was greater
300 than zero. Sites with significant delay- or array-related HFB power modulation were
301 identified using the second criterion applied to the respective epochs.
302
303 *Spatial tuning functions.* After identifying sites with significant task-evoked responses in
304 the HFB power of the IFPs for at least one peripheral location, we examined their

relative responses across all peripheral locations to determine their spatial tuning properties. In cases of spatial tuning, we defined a response field center (RF_C) as the location evoking the strongest power relative to baseline in response to the cue. Each site was considered to have a spatially-tuned IFP response field, if its tuning curve met three criteria. First, it had a significant task-evoked response at RF_C, as described above. Second, we determined whether the IFP responses were spatially selective by comparing the peak of the tuning curve (defined as RF_C) to the opposite location (RF_{null}) using a bootstrapped randomization. We generated a null distribution of randomized differences between RF_C and RF_{null} means by drawing with replacement from a pool of all RF_C and RF_{null} trials, including the number of RF_C trials in one mean and the number of RF_{null} trials in the other. The difference between these randomly generated means was added to a null distribution of randomized differences. The quantile of the real difference (RF_C – RF_{null}) in the null distribution of randomized differences was taken as the *p*-value of the real difference. We rejected the null hypothesis that activity in RF_C and RF_{null} trials were recorded from the same distribution of responses for *p*-values < 0.01. And third, we determined whether each tuning curve was well described by a Gaussian function, where the variance explained by the fit of a Gaussian function was greater than 60% ($r^2 > 0.6$). Since task-evoked responses were recorded at locations arranged around a circular array at a constant eccentricity of 7°, the measured widths were converted from degrees of visual angle (dva) to circular distance around the arc: $wid = dva \times 2\pi 7°/360$. A few sites were excluded due to exceptionally wide variance of the Gaussian fit (excluded if σ > 240 dva; N = 6). Across all sites that met these criteria, the median σ was 52 dva, which corresponds to an arc length of 6° (min = 2°,

max = 17°). Spatial tuning was similarly determined for delay and late array activity by comparing HFB responses when attention was directed to RF_C (or neighboring locations) as compared to RF_{null}. We refer to the spatial tuning properties during the delay as 'memory field', and those in response to the attended (vs. unattended) array as 'attention field' (see **Figure 3** for examples).

Spatial tuning functions were generated by centering the mean power at each location on RF_C, and the tuning width was measured as half the area under the normalized tuning curve. Since subjects had different numbers of cue locations, we found the cubic spline interpolation of each tuning curve using the least common multiple of the subjects' location counts, which allowed us to compare spatial tuning of HFB responses from all recording sites within a cortical area. Each tuning curve was then normalized to its peak. The population response is shown as the mean of the smoothed, normalized tuning curves within each area. Error bars correspond to the 95% confidence intervals of bootstrapped distributions generated by resampling 500 times with replacement from trials in each condition at each site.

Response onset latencies. For each electrode, the onset latency of HFB responses was measured as the time-to-half-peak at RF_C in response to the cue, following analytical steps as in Lee et al. (2007). We first smoothed the HFB time series of each trial at RF_C with an 8 ms σ Gaussian kernel. A distribution of baseline trial-wise means (blm) was generated by randomly selecting power values 1000 times from all the baseline times and trials, equivalent to the number of trials (Ntr) and times (Nti) at RF_C, then taking the

mean over the Ntr to generate a distribution of 1000 randomized baseline time series. The response peak was defined as the maximum at RF_C in the 50-250 ms following cue onset that was greater than 99.9% of the blm distribution ($p < 0.001$). To ensure that we measured elevated, increasing responses, we set the minimum response time (L_0) as the first time at least 50 ms after cue onset that the response was more than half the peak value. The response onset latency was then taken as the first time point between L_0 and 250 ms after cue onset that the power exceeded half the peak. Only sites with response onset latencies during this time period were considered to have cue-evoked responses. To compare array onset latencies to cue responses, we also performed this analysis using array-evoked activity in the attend-to-RF_{null} condition, defined below.

Attentional modulation: magnitude and topography of effects. To determine the strengths of attentional modulation during the delay and in response to the array, we compared mean HFB power from trials when attention was directed to RF_C (the attend-to-RF_C condition) to trials when attention was directed away from RF_C toward the opposite field location (the attend-to-RF_{null} condition). We compared these trial-wise means by calculating an attentional modulation index (MI) of the normalized means in each epoch. For each site, the time series of the responses in the attend-to-RF_C and the attend-to-RF_{null} conditions were normalized to the maximum value in the 500 ms window following cue onset (for delay effects) or array onset. The population time series for each area was the mean of these normalized time series across sites. The modulation index was the mean difference between the normalized attend-to-RF_C and the attend-to-RF_{null} time series in the time window of interest, yielding the proportion of the

maximum response. A distribution of bootstrapped MI values was found for each area by repeating the MI calculation 1000 times after resampling with replacement from trials in the attend-to-RF_C and attend-to-RF_{null} conditions.

MI values were determined for each site, and sites were assigned to an enhanced (MI > 0) or suppressed (MI < 0) group within each area, and then averaged across sites to yield population data. Note that the assignment of sites to these groups did not rely on a significance test, and was presumed to include noise around zero.

The MI values during the delay and in the late array window were mapped onto brain surfaces and combined across subjects onto a surface in common space to yield their topography. Specifically, electrode coordinates of each subject were first identified in their native brain space then realigned to a normalized brain. For sites with a response field, the topography of attentional modulation effects during the delay and late array windows across subjects were plotted in this common space with color indicating MI spread cortically using a Gaussian kernel of 4 cm. Large dots denote the topographic sites, and small dots the non-topographic ones.

Attentional modulation: latencies. Attentional modulation latencies were calculated based on the time courses of HFB responses evoked by the array in the attend-to-RF_C condition versus the attend-to-RF_{null} condition. Time series were averaged across recording sites from the same area with an enhanced (or separately for suppressed) modulation index to yield population data; the modulation latencies were determined

based on these population data. The modulation latency was defined as the first time point in a series of at least 50 consecutive milliseconds after the array onset latency (defined above as the time to half peak of the response at RF_{null}) during which the responses in the attend-to-RF_C condition were greater (or smaller in the case of suppressive effects) than in the attend-to-RF_{null} condition using the cluster method described below. Our approach is similar to other studies measuring attentional modulation latencies, using the first of several consecutive significant time points (e.g. Gregoriou et al., 2009; Buffalo et al., 2010); however, we required longer clusters of significance (50 ms compared to 30 ms) and smaller time bins (1 ms compared to 10 ms) due to the differences in signal quality in HFB power compared to spiking activity.

Tests of statistical significance. To compare effects between areas, we generated bootstrapped distributions of the population means across sites within each area by randomly resampling 500 times with replacement from the trials in each condition. For example, for tuning widths we resampled from trials at each cue location to generate a randomized mean for each site at that cue location, then took the mean across the sites in the area, repeated 500 times to generate a distribution across the population of sites in that area. Using these distributions, we compared the means between every area using ANOVA, and the significance of each difference was determined by applying the Holm-Bonferroni sequential correction for multiple comparisons on the resulting *p*-values. In this method, a single target alpha level is applied across the set of tests, yielding a single *p*-value for all tests. Across all comparisons, the *p*-values from the

ANOVA were ranked from the smallest to the largest and compared to a ranked alpha level determined by:

$$\alpha_{rank} = \frac{Target\ Alpha\ Level}{n - rank + 1}$$

where n was the number of tests, and the $Target\ Alpha\ Level$ was set as 0.05. For instance, 15 areas were included in the comparison of tuning widths (**Table 5**), so the number of tests n was $\binom{15}{2} = 105$. In order of their rank, if a test had $p - value_{rank} < \alpha_{rank}$ then that test was considered significant at the $Target\ Alpha\ Level$. The first test with $p - value_{rank} \geq \alpha_{rank}$ was not significant, as well as all subsequent tests.

To determine whether an effect within an area was significantly different from zero, we found the 95% confidence interval (CI) of the bootstrapped distribution. Areas with CI that did not overlap zero were significantly modulated ($p < 0.05$). We employed Spearman's rank correlation to determine the relationship between cue-evoked tuning widths and latencies.

For measurements of sustained cue-evoked activity, we used a non-parametric cluster method (Maris and Oostenveld, 2007) to determine the number of sequential time points with significant enhancement relative to baseline. With this method, we set a threshold for significance ($p < 0.05$) and found clusters of sequential time points after the cue onset latency with significantly elevated power at RF_C. We used the quantile of the RF_C power at each time point relative to a randomized distribution of baseline mean values as the test statistic at each time point. The cluster level statistic was the sum of the test statistics in the cluster. We compared veridical cluster level statistics to a null

441 distribution of cluster level statistics generated by randomly assigning time points as
442 event-related or baseline. Clusters of time points were significant if their veridical cluster
443 level statistic was greater than 99% of the randomly generated cluster level statistics in
444 the null distribution ($p < 0.01$).
445
446 To determine the attentional modulation latencies after array onset, we repeated the
447 assessment of sustained activity but used the time series after the array onset and
448 compared the attend-to-RF_C condition to the attend-to-RF_{null} condition rather than to
449 baseline. The latency of attentional modulation was the first time point of the first cluster
450 after the array onset latency when attend-to-RF_C was greater than attend-to-RF_{null} (or
451 smaller in the case of suppression effects).
452
453 Only areas with at least half of the bootstrapped calculations yielding a modulation
454 latency were included in the group-wise comparison, thus areas ISP4+, FEF, and the
455 non-topographic regions of occipital cortex were excluded from the group of modulation
456 latencies. For area V1d/v enhanced sites, the distribution of bootstrapped modulation
457 latencies was bimodal, so we separated the population of those latencies into two
458 groups, which had an early (V1c1) and a late (V1c2) component. The distributions for
459 V1c1 and V1c2 were used in the group-wise comparisons.
460

RESULTS

We recorded IFPs from 758 subdural electrodes implanted over parietal, occipital, temporal, and frontal cortex in 8 patients, who underwent pre-surgical epilepsy evaluation (**Table 1**, **Figure 1**), while performing a spatial attention task. We eliminated 122 electrode channels that were compromised due to noise or epileptiform activity, yielding 636 channels for analysis.

Electrode localization

In each patient, structural MRI and CT images of the implanted electrodes were used to reconstruct their locations in occipital (N = 54), temporal (N = 170), parietal (N = 280), and frontal cortex (N = 132). To relate electrode positions more specifically to topographically organized areas of the visual system, we combined the structural MRI of each individual patient with a probabilistic atlas of visuospatial topographic cortex (Wang et al., 2015). Electrode locations from all patients in relation to this probabilistic atlas are shown in **Figure 1**, rendered onto the left hemispheric surface of a standard brain and displaying posterior, lateral, and medial views. One hundred and thirty-three electrodes were located in the topographic visual system, including in early visual (V1-V3d/v, N = 36), dorsal extrastriate (V3A/B, TO1-2, N = 24), ventral extrastriate (hV4, LO1-2, VO1-2, PHC1-2, N = 24), and posterior parietal cortex, particularly in areas along the intraparietal sulcus (IPS; N = 42), as well as in the superior parietal lobule (SPL1, N = 3), and in frontal cortex (frontal eye fields, FEF, N = 4). The remaining 503 electrodes were implanted outside visuospatial topographic areas. Using the Harvard-Oxford parcellation that differentiates cortical areas using anatomical markers (Desikan

et al., 2006), these electrodes were broadly localized by lobe into occipital, temporal, parietal, and frontal categories. Since we did not find systematic differences in our analyses within a given category, results were combined by lobe (designated “Non-topographic, occipital” etc.). The electrodes in non-topographic cortex were distributed across parietal (N = 235), temporal (N = 134), and frontal lobes (N = 128), with only 6 electrodes in the occipital lobe located outside topographic cortex.

Task design and behavioral results

The patients were tested in a variant of the Eriksen flanker task (Eriksen and Eriksen, 1974; Eriksen, 1995), a classical spatial attention task that we also use in parallel monkey electrophysiology studies (Saalmann et al., 2012). Each trial of the task (**Figure 2A**) was initiated by an auditory tone and the presentation of a fixation point on a computer monitor. After a fixation period of 1100 ms, a cue was flashed briefly in a pseudo-randomly selected location arranged in a circular manner around the fixation point at a fixed eccentricity of 7°. The cue indicated with 100% validity the location of a subsequently presented target shape. After a variable delay period (300-700 ms), a circular array of barrel and bow tie shapes was presented, and the patients indicated with a left or right mouse button press which shape (i.e. barrel or bow tie) appeared at the cued location. Patients performed between 150 and 300 trials of this task (**Table 1**) and achieved high accuracies ranging from 83 to 96% (mean = 93±2%). Importantly, the patients showed the classical flanker effect, with higher accuracies for targets that were flanked by congruent shapes than targets that were flanked by incongruent shapes (congruent: mean = 96±2%, incongruent: mean = 90±3%, ttest $p < 0.04$). This

behavioral pattern indicates that the patients were engaged in the task and able to successfully perform it. In order to characterize the temporal dynamics of visual processing and its influences by attentional task demands, we report here on electrophysiological results from three epochs of the flanker task: cue-evoked (i.e., 'bottom-up' visual stimulation), delay period-related (i.e., maintenance of location information in the absence of visual stimulation), and array-evoked (i.e., the selection of behaviorally relevant stimuli among distracters).

Spatial selectivity of cue-evoked HFB response fields

We first examined the spatial selectivity of event-related power fluctuations of the intracranial field potentials (IFP) recorded from each electrode. A representative example of a response profile from an IFP evoked by cue stimuli is shown in **Figure 2**. The recording site was located in left dorsal V3 (cortical location shown in **Figure 3A**, electrode E). Cue-evoked power modulations (50-250 ms after the cue onset) were compared to a baseline period (200 ms before cue onset). Averaged across all trials, a cue-evoked enhancement in power was observed across a broad band of high frequencies (30-200 Hz) with a concomitant suppression of power in a narrow band of lower frequencies (7-20 Hz) (**Figure 2B**), similar to typical profiles of IFP power fluctuations in response to visual stimuli previously reported in ECoG studies (e.g. Lachaux et al., 2005).

By examining power modulations relative to baseline as a function of time, we found that cue and array stimuli evoked a robust increase in the high frequency broadband

(HFB) power with a precise temporal profile marking the onset of the visual stimulation (**Figure 2C**, **D** top panel; **Figure 3E**). In this report, we focus our analyses on modulations in HFB power between 70-200 Hz to exclude frequency bands that have been shown to have oscillatory properties such as gamma, beta, alpha or theta activity (Fries, 2009; Engel and Fries, 2010; Lisman and Jensen, 2013). However, control analyses on broadband activity that included gamma and beta frequency bands with the HFB responses yielded similar results. For the example electrode from dorsal V3, we sorted HFB responses in each trial based on cue location and found that the highest power was consistently evoked by the cue presented in positions 5 and 6 in the lower right quadrant (**Figure 2D**, center panel; **Figure 3E**, orange polar plot). Cues presented at locations further from the peak locations exerted continuously smaller HFB responses, thereby showing the typical profile of the cross section of a response field, which presents as a spatial tuning curve (**Figure 2D**, right panel). Thus, the visually-evoked increases in HFB power recorded from this site were highly spatially specific, constituting a contralateral ECoG HFB response field. We defined the location that evoked the strongest HFB responses as the response field center (RF_C) (**Figure 3E**, position 6) and the opposite field location as RF_{null} (**Figure 3E**, position 13). It is noteworthy that trial-wise responses for each cue position were reliable, with consistently stronger responses at RF_C (412% ± 32% of baseline, bootstrap randomization test $p < 0.001$) and consistently weaker or absent responses at the opposite field location (RF_{null}, 0.4% ± 3% of baseline, $p = 0.8$).

552 Cue-evoked HFB responses showed a high degree of spatial specificity across cortex,
553 both within topographic visual cortex and outside of topographic areas. We obtained
554 distinct spatial profiles even from adjacent electrodes, as illustrated in **Figure 3** for
555 electrodes that were part of a strip with 10 mm spacing. In addition to the example V3d
556 electrode (**Figure 3A**, electrode E), three nearby electrodes with ECoG HFB response
557 fields were implanted in areas IPS0 (**Figure 3A**, electrodes B and C, separated by 10
558 mm), and in V3B (**Figure 3A**, electrode D bordering V3A, separated from C and E by 10
559 and 14 mm respectively). We did not find HFB response fields in two other electrodes of
560 this strip (**Figure 3A**, blank circles). The peaks of the HFB response fields shifted from
561 position 5, just below the right horizontal meridian (**Figure 3B**) to position 3 in the upper
562 right quadrant (**Figure 3C**) within IPS0, and from position 3 in the upper right quadrant
563 within V3B (**Figure 3D**) to position 6 in the lower right quadrant of V3d (**Figure 3E**). This
564 topographic pattern of peak responses reflects the visual field sign reversals of the
565 underlying topographic maps (Wang et al., 2015; see also Konen and Kastner, 2008;
566 Silver and Kastner, 2009; Arcaro et al., 2011). Thus, HFB responses reflected activity
567 from spatially selective, local neuronal populations, and these signals did not appear to
568 be compromised by volume conduction from more distant sites (see Buzsáki et al.,
569 2012), corroborating and extending previous reports on the specificity of HFB responses
570 (e.g. Crone et al., 1998; Canolty et al., 2007; Parvizi et al., 2012). The spatial selectivity
571 of HFB responses across the human visual system formed the basis for our quantitative
572 analyses of the temporal dynamics and modulatory effects of selective attention on
573 baseline and visually-evoked activity.
574

575 Next, we determined the spatial tuning properties of cue-evoked HFB responses based
576 on the following criteria. First, for each recording site, we required responses to be
577 visually selective such that cue-evoked HFB power increased significantly relative to
578 baseline in response to at least one cue presentation location, as well as significant
579 differences between cue-evoked responses at the preferred location (RF_C) compared to
580 the opposite location (RF_{null}). Second, we required that the response profile of the
581 spatial tuning curve centered on RF_C had a regular shape (i.e., a Gaussian fit centered
582 on RF_C explained at least 60% of the variance, and the tuning widths were less than
583 240 degrees of visual angle). And third, in order to capture cue-evoked spatial tuning
584 only (and not delay-related tuning), we determined whether the response onset latency
585 at RF_C was within 50-250 ms of cue onset (latencies are discussed in detail below).
586
587 Using these criteria, 45% of electrodes located in topographic areas exhibited spatially-
588 tuned, cue-evoked responses (60/133) with a well-defined response field. The vast
589 majority of these had their RF_C in the contralateral hemifield (58/60, 97%). Additionally,
590 in ventral and dorsal parts of visual areas V1-V3, spatial tuning was predominantly
591 limited to the respective upper and lower visual field quadrants. Eighty-two percent, or
592 9/11 of the dorsal sites had their RF_C in the lower contralateral quadrant, and 2/2 of the
593 ventral sites had their RF_C in the upper contralateral quadrant. Of the recording sites
594 outside of topographic visual areas, 12% exhibited spatially tuned, cue-evoked HFB
595 responses (60/503), typically with their RF_C contralateral to the implanted hemisphere
596 (46/60, 77%). These sites were located in parietal (N = 35 selective, 27 with
597 contralateral RF_C), temporal (N = 14 selective, 12 with contralateral RF_C) and frontal

598 lobes (N = 11 selective, 7 with contralateral RF_C). Except if noted otherwise, only the
599 sites with a cue-evoked response field were included in further analyses.
600
601 **Cue-evoked response onset latencies**
602 We then examined the temporal dynamics of feedforward processing across the human
603 visual system by analyzing HFB cue response onset latencies at RF_C in topographic
604 and non-topographic areas. We defined onset latency as the time to half peak of the
605 power increase at RF_C in response to the cue (see Lee et al., 2007). For each recording
606 site, we compared the mean timeseries of HFB power at RF_C to a bootstrapped
607 distribution of baseline means, finding the peak power in the cue interval that was
608 greater than at least 99.9% of the bootstrapped baseline distribution. The onset latency
609 was taken as the first time point at which the power was greater than half the peak. In
610 the example area V3d electrode, the cue-evoked responses at RF_C were highly
611 consistent across trials and had a reliable onset latency of 59±8 ms (**Figure 2D**, top
612 panel). As expected from monkey single-unit recording studies (e.g. Schmolesky et al.,
613 1998), HFB latencies increased systematically across the ventral and dorsal processing
614 pathways (**Figure 4**; **Tables 2**, **3**).
615
616 Response onset latencies increased along the dorsal pathway from early visual areas
617 (V1-V3d/v mean = 73±4 ms) to dorsal extrastriate areas (V3A/B and TO1-2 mean =
618 107±9 ms, $p < 0.05$, see **Table 3** for all area-wise comparisons) and IPS0 (106±5 ms).
619 IPS0 latencies were faster than those in more anterior IPS areas. Response onset
620 latencies in the ventral pathway were quite long, with ventral extrastriate area

responses (mean = 149±5 ms) on the order of those in the anterior IPS, and slower than in dorsal extrastriate and posterior IPS. These findings were not only observed in the population data, but they were remarkably consistent across the 4 individual patients with extensive electrode coverage of the visual system (results not illustrated). Interestingly, as in previous monkey studies (Schmolesky et al., 1998), area FEF had a fast latency of 62±5 ms, on the order of the population latencies in early visual cortex. This fast latency likely reflects projections from the superior colliculus that bypass the cortex. Although this latency was obtained from only two sites, these fast latencies were quite consistent (**Figure 4C**), and they were recorded from two patients (S3 and S6). Conduction delays between subsequent processing stages along the dorsal pathway were estimated to be on the order of ~15 ms by examining the progression from V1-V2-V3-V3A-IPS0 (see **Table 2**). In non-topographic sites, response onset latencies in the frontal (84±5 ms), parietal (100±3 ms), and temporal lobes (109±5 ms) were slower than early visual areas and faster than the anterior topographic IPS and ventral extrastriate areas (**Figure 4C**).

To determine whether the cue onset latencies were biased by particular stimulus properties such as shape and size, we also compared array onset latencies of trials in which attention was not at RF_C (the attend-to-RF_{null} condition) to the cue onset latencies, and found no differences in latencies across the topographic areas (ttest, p = 0.6). Thus, response onset latencies did not appear to depend on the different stimulus configurations used in our study.

644 Taken together, the temporal dynamics of cue-evoked responses along the dorsal and
645 ventral visual pathways were consistent with the notion of a hierarchical feedforward
646 architecture of visual processing.
647
648 **Attentional modulation effects and their topography**
649 In order to determine dynamic task-related modulations of visual processing and probe
650 feedback effects, we examined attention effects on baseline activity in the absence of
651 visual stimulation (i.e. during the delay) and in response to the array by comparing
652 responses from trials when attention was allocated at RF_C to trials when attention was
653 allocated at RF_{null}, similar to approaches typically taken in monkey physiology studies
654 (e.g. Reynolds and Chelazzi, 2004). First, we characterized the different types of
655 attentional modulation and their topography across the human visual system and non-
656 topographic cortex. The vast majority of attention effects were enhancement of HFB
657 responses during the delay and in response to the array, as shown for an example
658 electrode located in area TO and for the TO population response in **Figure 5** (upper
659 panels). Such enhancement effects were not only observed at RF_C, but typically had a
660 spatial extent that was similar to the cue-evoked HFB response field, as can be seen in
661 the examples shown in **Figure 3** (modulation of array-evoked responses: solid purple
662 plot; modulation of responses during delay: dashed purple plots). Collectively, the
663 modulation at the different spatial locations relative to the response at RF_{null} gave rise to
664 an 'attention field'. Similarly, response enhancement during the delay was spatially
665 tuned and gave rise to a 'memory field' (see below for further results).
666

667 Attention and memory fields were observed in many extrastriate sites but were
668 markedly absent in early visual cortex (**Figure 6**), especially during the delay. Of the
669 sites in early visual cortex that had a response field, only one site showed significant
670 attentional modulation during the delay (N_{delay} = 1/13, 8%). Ventral extrastriate areas
671 also had a low proportion of sites with a significant delay enhancement effect (N_{delay} =
672 2/11, 18%). In comparison, in dorsal extrastriate and IPS areas about 50% of sites
673 showed significantly enhanced delay activity (dorsal extrastriate N_{delay} = 5/11, 45%;
674 IPS0-2 N_{delay} = 6/12, 50%; IPS3-5 and SPL1 N_{delay} = 6/11, 54%). Among non-
675 topographic areas, 20% of the sites that showed cue-evoked spatial tuning exhibited
676 significant modulation of activity during the delay (N_{delay} = 12/60). Early visual areas also
677 had relatively few sites with a significant effect of attention in response to the array
678 (N_{array} = 5/13, 38% in the late array period) compared to dorsal extrastriate areas and
679 posterior IPS which had a high proportion with a significant attentional enhancement
680 during the late array period (V3A, V3B, TO1-2 N_{array} = 7/11, 64%; IPS0-2 N_{array} = 7/12,
681 58%).
682
683 It is notable that the topography of attentional enhancement effects during the delay and
684 in response to the array was not identical (**Figure 6**; red colors). In particular, although
685 ventral extrastriate areas LO/VO had a low proportion of sites that showed significant
686 enhancement during the delay (18%), these areas had a majority of sites showing an
687 enhancement effect in response to the array (N_{array} = 7/11, 64%). In non-topographic
688 parietal areas, only 15% of sites showed enhanced delay activity (N = 9/60), while 40%
689 exhibited attentional enhancement in response to the array (N = 24/60). Conversely,

690 while anterior IPS areas IPS4+ had a high proportion of sites with a significant effect
691 during the delay (54%), it had only few sites with significant enhancement in response
692 to the array (N_{array} = 3/11, 27%). Thus, only dorsal extrastriate areas and posterior IPS
693 had a majority of sites enhanced by attention during both the delay and in response to
694 the array (dorsal extrastriate: delay 45%, array 64%; IPS0-2: delay 50%, array 58%).
695
696 We also observed attentional suppression effects during the delay or in response to the
697 array, albeit less frequently (**Figure 6**; green colors). The example electrode shown in
698 **Figure 5** (mid-left panel) was located in V1 and showed a reduction of about 50% in
699 HFB responses to the array when attention was directed to RF_C as compared to RF_{null}.
700 Attentional suppression has been previously observed in monkey physiology studies as
701 a decrease of LFP power and spike-field coherence in gamma frequency bands (40-60
702 Hz; Chalk et al., 2010). Given that we used an array of stimuli it is likely that inhibitory
703 center-surround interactions and top-down influences contributed to these effects (Ito
704 and Gilbert, 1999; Angelucci et al., 2002; Bair et al., 2003; Ozeki et al., 2009; Zhang et
705 al., 2014; Cox et al., 2017). A similar result was obtained for the population of V1d/v
706 sites, with an overall suppression effect of about 10% in response to the array (**Figure**
707 **5**, mid-right panel). Attentional suppression effects were also found in IPS areas (**Figure**
708 **6**; green colors). Interestingly, array-related suppression in IPS could be observed with
709 elevated delay activity, as shown in **Figure 5** (lower left panel) for an electrode located
710 in area IPS3 (see also the blue arrows for sites with such effects, **Figure 6A** and **B**).
711 Since both array-related attentional enhancement and suppression effects were found

712 in this area, no net effect of modulation resulted in the population response (**Figure 5**,
713 lower right panel, mean = 5±6% enhancement, bootstrap randomization test $p = 0.06$).
714
715 **Strengths of attentional modulation effects**
716 Hierarchical top-down models assume modulatory attention effects to reverse the
717 bottom-up processing hierarchy. One prediction of such a model is that effects of
718 attention are stronger at advanced as compared to early stages of visual processing.
719 Therefore, we probed the strengths of modulatory effects across the human visual
720 system as well as in non-topographic cortex. We quantified the attention effects
721 obtained during the delay and in response to the array using a modulation index (MI;
722 defined as the difference between the mean power in attend-to-RF_C and attend-to-RF_{null}
723 conditions, normalized to the maximum response). The MI therefore calculates the
724 modulation effect as the proportion of the maximum HFB response. We calculated the
725 MI for the delay period (200 ms before array onset, only including trials with cue-target
726 intervals greater than 450 ms to capture attention effects that were not contaminated by
727 cue-evoked responses), early array (50-200 ms), and late array period (300-500 ms).
728 Positive values indicate enhancement effects (shown in red colors in **Figure 6**) and
729 negative values indicate suppression effects (shown in green colors in **Figure 6**).
730
731 To compare the effects of attention between areas, we separately generated
732 bootstrapped distributions of MIs using the population of sites with either enhanced or
733 suppressed effects in each area. Importantly, sites were not assigned to those groups
734 based on any measure of significance, but strictly based on whether their MI was

positive or negative. Statistical analyses for each area were then performed on the population means of each of those groups. During the delay, we found significant enhancement effects of attention in dorsal and ventral extrastriate areas (V3A, TO1-2, LO1-2, hV4, VO1-2), as well as in IPS areas IPS0-3 (bootstrap randomization test, each $p < 0.001$) (**Figure 6A** red colors, **7A**). No significant enhancement effects were found in early visual areas V1d/v, V2d/v, or V3d/v, nor in dorsal extrastriate area V3B or anterior IPS areas IPS4-5, SPL1, and FEF (each $p \sim 0.1$) (**Figure 6A** red colors, **7A**). Of the areas with a significant effect, V3A (MI_{delay} = 12±8%, N = 3) and LO (MI_{delay} = 20±14%, N = 8) showed weaker modulation during the delay than IPS areas (IPS0: MI_{delay} = 23±8%, N = 8; IPS1-2: MI_{delay} = 28±16%, N = 2; IPS3: MI_{delay} = 24±8%, N = 7) and dorsal extrastriate area TO (MI_{delay} = 37±17%, N = 3). The significance of each comparison is shown in **Table 4**.

Outside visual topographic cortex, we found significant population enhancement effects in parietal (MI_{delay} = 34±10%, N = 23), frontal (MI_{delay} = 33±16%, N = 7), and temporal lobes (MI_{delay} = 25±16%, N = 8) (each $p < 0.001$) (**Figure 6A** red colors, **7A**), with modulatory effects similar in strength to higher order topographic areas (**Table 4**).

Of the sites with a negative MI, attention significantly suppressed HFB power modulations in the population of V1d/v (MI_{delay} = 11±7%, N = 3), ISP4+ (MI_{delay} = 33±27%, N = 1), and non-topographic temporal lobe sites (MI_{delay} = 21±18%, N = 6) (bootstrap randomization test, all $p < 0.001$) (**Figure 6A** green colors, **7A**). Notably, although the positive effects were not always significant in these areas, when we

examined the effect across all sites in each area we found no *overall* effect of attention during the delay (V1d/v $p = 0.06$, IPS4+ $p = 0.4$, non-topographic temporal sites $p = 0.8$).

Next, we investigated attentional modulation of array-evoked activity. Attention effects can typically be observed in later time windows, since the feedforward cascade of visual stimulation strongly activates sites within the visual system regardless of whether they are attended to or not. For the time period of 300-500 ms after array onset, we found significant positive modulation effects in early, dorsal and ventral extrastriate visual areas ($p < 0.001$), as well as consistently strong effects in IPS areas ($p < 0.001$) (**Figure 7C**). The strength of the modulation generally increased across the cortical hierarchy through IPS0, with the weakest modulation in early visual areas (V1d/v MI_{array} = 15±7%), and the strongest modulation in dorsal extrastriate area TO (MI_{array} = 40±14%), ventral extrastriate areas LO/VO (MI_{array} = 40±7%), and posterior parietal area ISP0 (MI_{array} = 53±7%) (**Figure 6B** red colors, **7C**; significance of all comparisons shown in **Table 4**). Interestingly, the anterior IPS areas were as weakly modulated as early visual area V1d/v (IPS4+ MI_{array} = 16±10%) (**Figure 7C**, **Table 4**). We also observed significant suppression in areas V1d/v and IPS3 (MI_{array} = -27±9% and -25±14%, respectively) (**Figure 7C**), which were the only areas with this effect either across the population or from individual sites (sites with significant array suppression in V1d/v, N_{array} = 2 from patient S1; IPS3, N_{array} = 1 from S5). In contrast, during the early array period, when attention effects and visual onset activity interact, only topographic areas TO, IPS0-2, and LO/VO were significantly modulated (bootstrapped mean±95%CI, TO

781 MI_{array} = 41±14%; IPS0 MI_{array} = 14±7%; IPS1-2 MI_{array} = 22±14%; LO/VO MI_{array} =
782 18±8%) (**Figure 7B**).
783
784 In summary, TO, IPS0-2, and LO/VO exhibited stronger attentional modulation effects
785 than early visual and anterior IPS areas both during the delay and in the late array
786 window, and these were the only topographic areas that were significantly modulated
787 during their early response to the array. While the stronger attention effects in
788 extrastriate and posterior parietal cortex relative to early visual cortex are consistent
789 with hierarchical top-down models of attention, the weak or absent attention effects in
790 the anterior IPS and frontal cortex, particularly during visual processing, are in conflict
791 with such models.
792
793 **Attentional modulation latencies**
794 Just as the temporal order of visual onset responses informs about the temporal
795 dynamics of feedforward visual processing, the timing of selective processing after the
796 array onset provides insight into the temporal dynamics of feedback attentional
797 modulation. Hierarchical top-down models predict that the latencies of attentional
798 modulation systematically increase from advanced to early processing stages as a
799 further indication for a reversal of the processing hierarchy during attentional selection.
800 To determine the latency of attentional modulation after array onset, we examined the
801 population time courses of each area sorted by modulation effects (i.e. enhancement or
802 suppression based on each sites' MI in the late array window). First, we determined
803 which time points showed a significant effect of attention in response to the array

804 (attend-to-RF_C > attend-to-RF_{null}, bootstrap randomization $p < 0.05$). Then, we identified
805 clusters of consecutive significant time points after array onset that lasted for at least 50
806 ms (Maris and Oostenveld, 2007). The first time point in the first cluster of significant
807 ones after array onset was defined as attentional modulation latency (see Methods for
808 more details). To compare latencies across areas, we generated bootstrapped
809 distributions of attentional modulation latencies by resampling 500 times, with
810 replacement, from trials in each condition by site and recalculating the latency based on
811 that set of trials. We determined whether two areas had significantly different latencies
812 by comparing the population means of the distributions, then applying Holm's sequential
813 Bonferroni correction for multiple comparisons at alpha level $p < 0.05$ across all the
814 comparisons. The results are summarized in **Tables 2** and **3**.
815
816 Consistent with the idea that feedback signals are generated in higher order cortex and
817 modulate early sensory processing areas via cortico-cortical feedback, we found that
818 modulation latencies were longest in early visual cortex (**Figures 8**, **9** and **Tables 2**, **3**).
819 Modulation latencies were slowest in V1d/v (late component, 315±33 ms), followed by
820 V2d/v (295±16 ms), V3d/v (233±12 ms), V3A (246±8 ms), and V3B (268±22 ms)
821 (significance of all comparisons shown in **Table 3**). The attentional modulation latencies
822 in posterior IPS (IPS0: 156±18 ms, IPS1-2: 119±22 ms), dorsal extrastriate area TO1-2
823 (129±3 ms) and ventral extrastriate areas LO/VO (172±7 ms) were significantly faster
824 than those in early visual areas. However, the modulation latency in area IPS3, located
825 anterior to IPS0-2, was significantly longer than the latencies in the posterior IPS and on
826 the order of latencies in early visual areas (IPS3 latency = 225±11 ms; **Figures 8**, **9** and

827 **Tables 2**, **3**). Although the more anterior IPS areas of IPS4+ had significant modulation
828 effects (**Figure 7C**), the responses were not robust across trials and sites, yielding less
829 than 50% of bootstrapped time series with a significant modulation effect. Therefore, the
830 latencies calculated in this area were not considered significant (see Methods).
831 However, it is worth mentioning that the trend of increasing latencies through the higher
832 order IPS areas continued in IPS4+: of the bootstrapped time series where we were
833 able to determine a modulation effect, the latency was even slower than IPS3 and on
834 the order of the slow V1d/v effects (latency = 352±22 ms from 41% of the bootstrapped
835 time series). Further, modulation latencies could not be determined in FEF due to the
836 absence of modulation effects (**Figure 7**). Thus, the pattern of attentional modulation
837 latencies did not strictly follow the concept of top-down feedback from higher to lower
838 order cortex, with the fastest latencies found instead in intermediate areas of the
839 processing streams.
840
841 In V1d/v, we found that the distribution of modulation latencies was bimodal, reflecting
842 two components (**Figure 9B**, red traces). A fast component indicated the effect of
843 attention as early as 80 ms in V1 after array onset (83±9 ms) (**Figure 8**, V1), which was
844 the fastest effect of attentional enhancement that we observed across all areas.
845 Although these responses are too fast to reflect cortico-cortical feedback modulation,
846 they are consistent with the very fast attention latencies reported in LGN magnocellular
847 populations (McAlonan et al., 2008), suggesting that a feedforward attentional
848 modulation may be passed onto V1 from LGN. We also measured the response onset
849 latencies of the suppression effects (**Figure 7C**). In V1d/v, the suppression effect was

even earlier than the fast component of the enhanced responses (68±7 ms, bootstrap randomization $p < 0.01$). The suppression effects in IPS3 sites with a negative MI were late (265±142 ms), on the order of the late enhancement effects found in IPS3 ($p = 0.7$).

Outside the topographic areas, parietal lobe sites had fast modulation latencies similar to those observed in IPS0 and IPS1/2 (124±7 ms), and temporal lobe sites had modulation latencies on the order of those in ventral extrastriate areas (223±16 ms).

In a further test of the effect of attention on response onset latencies, we examined whether array onset responses were faster with attention. Previous studies of response onset latencies in extrastriate cortex of macaques had found a small, but consistent lag in response to ignored stimuli (Sundberg et al., 2012). However, we did not observe any systematic increases or lags in onset latencies with attention across the topographic areas (ttest $p \sim 0.6$).

Spatial tuning of response, memory, and attention fields

Although our task was not designed to probe spatial tuning properties systematically and in detail (e.g. such as a function of eccentricity), we examined spatial tuning properties at a fixed peripheral eccentricity (i.e., 7°, which was the constant eccentricity at which the cue was presented) across the human visual system as well as outside of topographic visual cortex. Across all recording sites in each area that exhibited cue-evoked, spatially-tuned HFB response fields, we determined the population HFB spatial tuning curves (**Figure 10A**), and the population widths at half height of the tuning curves

873 (**Figure 10B**), as well as their individual distributions by area (**Figure 10C**; see Methods
874 for further details). We compared the tuning widths between the areas by generating
875 bootstrapped distributions of mean tuning widths in each area after resampling, 500
876 times, from trials in each condition. The significance of the differences between these
877 bootstrapped distributions was determined by applying the Holm-Bonferroni sequential
878 correction for multiple comparisons at the target alpha level of $p < 0.05$ (see Methods).
879 As expected from a wealth of fMRI studies in humans and electrophysiology studies in
880 monkeys (e.g. Felleman and Van Essen, 1987; Dumoulin and Wandell, 2008; Wandell
881 and Winawer, 2015), spatial tuning widths increased systematically across both the
882 dorsal and ventral visual processing pathways (**Figure 10**, **Table 5**). This progression
883 was apparent in the population data (**Figure 10B**), as well as in the distribution of tuning
884 widths from individual recording sites (**Figure 10C**). Early visual areas V1-V3d/v had
885 significantly narrower tuning widths (mean = 9.5±0.1°, N = 13) than dorsal extrastriate
886 areas (V3A/B and TO1-2 mean = 13.1±0.2°, N = 12; $p < 0.05$, see **Table 5** for all area-
887 wise comparisons) and ventral extrastriate areas (LO1-2, hV4, and VO1-2 mean =
888 13.2±0.4°, N = 11). Dorsal and ventral extrastriate areas were in turn more sharply
889 tuned than posterior and anterior IPS areas (IPS0-2 mean =15.5±0.5°, N = 12; IPS3-5
890 and SPL1 mean = 15.8±0.6°, N = 11). Tuning widths of areas along the IPS were
891 comparable. Non-topographic sites had tuning widths similar to higher order
892 topographic areas, with parietal lobe sites' tuning widths on the order of the topographic
893 IPS sites (mean = 14.4±0.2°, N = 35), and temporal lobe sites' widths comparable to the
894 dorsal and ventral extrastriate sites (mean = 11.9±0.7°, N = 14).
895

We also determined the spatial tuning widths during the delay period ('memory field') and in response to the array ('attention field'). At individual sites, a general broadening of the attention fields relative to the cue-evoked response fields was observed (**Figure 3**, **B-E** purple compared to orange polar plots). At the population level, we investigated the effect of attention on the response field widths by examining the population of sites in each area that had a significant population enhancement effect (sites from areas with a significant positive MI in **Figure 7**). We generated trial-wise bootstrapped distributions of mean memory and attention fields, from which we calculated the widths during the delay and in the late array window. We found that memory fields were significantly broader than response fields in TO1-2 and ventral extrastriate areas (increase of 2.7±0.3% and 7.5±0.5%, respectively; bootstrap randomization test $p < 0.001$), as well as the non-topographic areas (mean increase = 8.6±0.5%, $p < 0.01$). In contrast, we did not find significant differences in response and memory field widths in area V3A, nor the IPS areas IPS0-3 ($p \sim 0.1$) (**Figure 11A**).

All of the topographic areas that were significantly enhanced by attention (positive MI in **Figure 7C**) showed increased attention field widths relative to their respective cue-evoked response fields (**Figure 11B**). The effect was remarkably similar across the topographic areas, suggesting a global effect of attentional modulation on visual space, consistent with a recent fMRI study (Klein et al., 2014). Except for areas V1d/v and V3d/v, which had spatial attention field widths about 8% broader than their response fields, all other topographic areas and the non-topographic sites showed broadening of spatial attention tuning widths on the order of 3% (mean increase = 2.6±0.3%, all $p <$

0.001). Such broadening may be due to expansion of RFs, as observed in single neurons when attention is allocated next to the RF (Anton-Erxleben et al., 2009). At the same time, there is also evidence that RFs shrink in extent when attention is allocated (e.g. Womelsdorf et al., 2006). Reconciling these contradictory observations with our findings may imply that, at the intracranial field potential (IFP) spatial scale, the overall effect appears to be broadening of the IFP response field due to the many contributing individual neurons' RFs expanding and only a smaller number of individual neurons' RFs shrinking. Such broadening appears to occur only in response to visual stimuli, since we did not observe the same effect for memory fields. Relative to the memory field widths, attention fields were broader in areas TO1-2, IPS1-2, and IPS3 ($p < 0.001$), narrower in ventral extrastriate areas LO/VO and non-topographic areas ($p < 0.001$), and similar in V3A and IPS0 ($p = 0.4$) (**Figure 11C**).

DISCUSSION

We analyzed HFB responses from intracranial recordings of 626 electrodes implanted in 8 epilepsy patients, who performed a spatial attention task, in order to characterize a dynamic visual processing architecture, modulated by attentional task demands, in the human brain. Electrode locations were reconstructed using a probabilistic atlas of the human visual system (Wang et al., 2015). HFB responses showed high spatial selectivity and tuning, constituting ECoG response fields (RFs) that were found within and outside the topographic visual system. Both RF widths and onset latencies increased systematically across the visual processing hierarchy. We utilized the spatial specificity of ECoG responses to quantitatively study spatial attention effects on baseline and visually-evoked activity. Attention effects were stronger, and attention modulation latencies were shorter, in extrastriate, and posterior parietal cortex than in early visual cortex. However, attention effects in anterior IPS and frontal cortex were weaker, and modulation latencies in anterior IPS were longer, than in posterior IPS. Together, the temporal dynamics and modulatory effects of spatial attention revealed in these studies only partially support attentional top-down models that assume a reversal of the visual processing hierarchy.

The electrophysiological basis of HFB responses is still an area of active investigation. HFB power fluctuations have been shown to correlate with multi-unit activity from large populations of neurons in the vicinity of the recording electrode (Ray et al., 2008a; Ray and Maunsell, 2011; Rich and Wallis, 2017; Watson et al., 2018). More recent findings indicate CA+ dendritic spikes in supragranular cortex as a principle contributor to pial

HFB responses (Leszczyński et al., 2018). However, models of HFB responses have also shown that power increases are predicted by increases in neuronal synchronization (Ray et al., 2008a). The underlying firing patterns may consist of multiple band-limited neuronal oscillations at different peak frequencies within the gamma band (Crone et al., 2011). Thus, it is possible that HFB responses index to some extent neuronal synchronization. We utilized the high spatial and temporal precision of HFB responses to track the temporal dynamics of visual and attentional processing.

Spatial specificity of ECoG response fields

Similar to previous reports from human early visual cortex (Yoshor et al., 2007; Winawer and Parvizi, 2016) and monkey visual cortex (Bosman et al., 2012), we found spatially confined ECoG RFs based on cue-evoked HFB responses. The spatial configurations of the RFs reflected the visual field representations of the underlying maps that are known from fMRI studies (Wang et al. 2015; see also Konen and Kastner, 2008; Silver and Kastner, 2009; Arcaro et al., 2011). Remarkably, electrodes that were located as little as 1 cm apart showed visual field sign reversals along the horizontal meridian with RF peaks in the upper and lower quadrants, respectively, underlining the impressive specificity of HFB responses, shown in several other domains (e.g. Crone, 1998; Canolty et al., 2007; Parvizi et al., 2012; Daitch et al., 2016). Interestingly, a large proportion of electrodes with ECoG RFs was found outside topographic cortex, equally distributed across the major lobes. The identification of spatially-selective, but relatively isolated sites outside of visual maps is difficult with techniques such as MEG/EEG and

977 fMRI, which have a poor signal-to-noise ratio. Thus, spatially selective responses
978 appear to be surprisingly ubiquitous outside of the topographic visual system.
979
980 **Temporal dynamics of feedforward processing**
981 This is the first report of systematic HFB response onset latencies across the human
982 visual system (see Yoshor et al., 2007 for LFP onset latencies). Onset latencies
983 increased gradually across the dorsal processing pathway, where we had systematic
984 coverage, with estimated conduction delays of 10-15 ms between areas. Responses in
985 V1 were recorded as fast as 50 ms after stimulus onset. In general, these results are in
986 excellent agreement with monkey physiology studies (e.g. Schmolesky et al., 1998).
987 Notably, we also found extremely short latencies in FEF that were comparable to the
988 onset latencies in early visual cortex. However, a few of our findings were not
989 predictable from what is known about the monkey visual system and therefore may be
990 unique features of the human visual system. First, in humans, onset latencies in TO (the
991 human MT/MST complex) were well above 100 ms and significantly longer than those in
992 other dorsal extrastriate areas such as areas V3d/v, or V3A. In contrast, in the monkey,
993 onset latencies in these areas are typically shorter and similar to one another (~70 ms;
994 Schmolesky et al., 1998; but see large range in Raiguel et al., 1989 and Azzopardi et
995 al., 2003). Second, onset latencies between higher-order dorsal and ventral extrastriate
996 areas, IPS1-4 and LO/VO were similar in humans. In contrast, onset latencies between
997 dorsal and ventral higher-order cortex differ significantly in monkeys due to the relatively
998 greater magnocellular input to the dorsal pathway. For example, neurons in LIP respond
999 to shape stimuli with a latency of ~60 ms, whereas neurons in anterior inferotemporal

cortex will respond after ~100 ms (Lehky and Sereno, 2007). This discrepancy, as well as the longer latencies in TO, may be attributable to the greater capacity of the human dorsal pathway to represent shape and object information (Konen and Kastner, 2008; Freud et al., 2016; Kastner et al., 2017). FMRI studies have shown that the human ventral and dorsal visual pathways represent non-spatial shape and object information similarly (Konen and Kastner, 2008), and thus the human dorsal pathway must receive a relatively greater input from the slower parvocellular system as compared to the monkey dorsal pathway, which in turn might explain the longer onset latencies in TO and IPS. Despite these notable human-specific features in the dynamics of feedforward processing, as indexed by response onset latencies, our results provide strong support for a hierarchical visual processing architecture in the human brain.

Spatial attention effects and modulation latencies

The temporal dynamics and strengths of attentional modulation have been interpreted as evidence in support of a top-down feedback model of selective attention. Specifically, monkey physiology studies have shown that attentional modulation latencies were shorter and the strength of attentional modulation was greater in higher-order cortex than in lower-order cortex. For example, Buffalo et al. (2010) recorded from areas V1, V2, and V4 and found that attention effects reversed modulation strengths and temporal order such that attentional enhancement was found to be larger and earlier in V4 and smaller and later in V1, with V2 showing intermediate results, similar to earlier findings by Mehta et al. (2000). These studies have provided support for the idea of a backward propagation of attentional feedback signals across the visual processing hierarchy.

1023 We found widespread spatially-selective attention effects on HFB responses both on
1024 baseline activity during the delay and in response to the array, thereby corroborating
1025 previous ECoG studies on selective sensory processing (Szczepanski et al., 2010;
1026 Davidesco et al., 2013; Ray et al., 2008b; Golumbic et al., 2013). In accordance with a
1027 large body of literature from monkey physiology (e.g. Luck et al., 1997; Cook and
1028 Maunsell, 2002) and human brain imaging (e.g. O'Connor et al., 2002; Siegel et al.,
1029 2008), attentional modulation was generally stronger in higher-order compared to lower
1030 order areas.
1031
1032 Specifically, our recordings focused on a multitude of areas along the dorsal processing
1033 pathway. We found indeed a systematic 'backward propagation' in early visual cortex,
1034 from areas V3 to V2 and V1 with increasingly longer attentional modulation latencies,
1035 and these latencies were also significantly longer than those obtained in dorsal
1036 extrastriate cortex. However, the temporal dynamics in dorsal extrastriate and posterior
1037 parietal cortex were more complex. For example, area TO and IPS0 had significantly
1038 faster latencies than IPS3. Thus, these modulation latencies did not appear to follow a
1039 strictly hierarchical processing that was reversed during spatial attention and they do
1040 not lend unequivocal support for the top-down feedback model. However, our
1041 assumptions on the visual processing hierarchy along the human dorsal pathway can
1042 only be tentative. Based on the anatomical locations of areas, one would assume that
1043 TO projects to and receives feedback from the IPS areas, and the same would hold for
1044 the posterior relative to the anterior IPS areas, but detailed anatomical studies on
1045 structural connectivity are lacking. Connectivity – both structurally and functionally –

may be increasingly more divergent in higher-order cortex, thereby promoting parallel rather than hierarchical processing. For example, anterior IPS shows grip- and reach-related activations (Konen et al., 2013) as well as representations of tool and manipulable object information (Mruczek et al., 2013). Further, posterior IPS, but not IPS3-5, has been reported to interact with other fronto-parietal attention areas, like FEF and SEF, in visuospatial attention tasks (Szczepanski et al., 2013). Anterior IPS may thus contribute to a different network than posterior IPS, which may predominantly serve visuospatial attention and oculomotor functions. Interestingly, based on analyses of directed feedforward and feedback signaling indexed by synchronization in certain frequency channels, Michalareas et al., (2016) placed the anterior IPS areas below the posterior IPS areas in their functional hierarchy, which is further evidence for the more complex inter-areal dynamics during attentional processing particularly in human parietal cortex. Further, it is noteworthy that cortical network interactions are influenced by additional sources such as thalamic nuclei, which complicates the interpretation of temporal cortico-cortical interactions (see Halassa and Kastner, 2017 for an extensive discussion of alternative attention control models).

Attentional modulation in V1

Attention effects on array-evoked activity were moderate in early visual cortex. Both enhancement and suppression effects were found in V1, without a net effect of attention. The strongest attention effect that we obtained in V1 was attentional suppression, likely due to modulation of activity in extra-RF surrounds. These findings are consistent with previous monkey physiology studies that have shown attention-

1069 related decreases in LFP gamma power in the 40-60 Hz frequency band and spike-field
1070 coherence in V1 using stimuli that engaged suppressive extra-RF surrounds (Chalk et
1071 al., 2010), as well as with findings of attention-related increases of LFP gamma power
1072 when extra-RF surrounds were less stimulated (Bosman et al., 2012). Thus, it is
1073 possible that HFB responses also reflect neuronal synchronization processes, since
1074 attention-related modulation of spiking activity is typically moderate (Motter, 1993; Luck
1075 et al., 1997; McAdams and Maunsell, 1999; Grunewald et al., 2002; Marcus and Van
1076 Essen, 2002; see also, Yoshor et al., 2007).
1077
1078 Interestingly, we also found evidence of attentional feedforward modulation in V1, where
1079 three modulatory temporal components were found, two early components that were
1080 observed at array onset of attentional suppression and enhancement, and a late
1081 component that was observed with attentional enhancement and followed the top-down
1082 feedback model, discussed above. In monkey physiology studies, attentional
1083 feedforward modulation has been found in LGN and TRN (McAlonan et al., 2008). This
1084 modulation may be mediated through direct influences of prefrontal cortex on the TRN
1085 that bypass cortico-cortical feedback, as shown in the mouse model (Wimmer et al.,
1086 2015). The feedforward modulation observed in LGN-TRN may be passed on to V1 and
1087 thus account for our observations. In human EEG studies, attention effects on the
1088 earliest component (the ‘C1’; ~50 ms onset) that is typically attributed to a generator in
1089 striate cortex have been controversial (Martinez et al., 1999; Di Russo et al., 2003; Kelly
1090 et al., 2008). Our findings of two early components support the possibility that the
1091 earliest EEG component may be modulated by spatial attention.

REFERENCES

Angelucci, A., Levitt, J. B., Walton, E. J., Hupe, J. M., Bullier, J., & Lund, J. S. (2002). Circuits for local and global signal integration in primary visual cortex. *Journal of Neuroscience, 22*(19), 8633-8646.

Anton-Erxleben, K., Stephan, V. M., & Treue, S. (2009). Attention reshapes center-surround receptive field structure in macaque cortical area MT. *Cerebral Cortex, 19*(10), 2466-2478.

Arcaro, M. J., Pinsk, M. A., Li, X., & Kastner, S. (2011). Visuotopic organization of macaque posterior parietal cortex: a functional magnetic resonance imaging study. *Journal of Neuroscience, 31*(6), 2064-2078.

Azzopardi, P., Fallah, M., Gross, C. G., & Rodman, H. R. (2003). Response latencies of neurons in visual areas MT and MST of monkeys with striate cortex lesions. *Neuropsychologia, 41*(13), 1738-1756.

Bair, W., Cavanaugh, J. R., & Movshon, J. A. (2003). Time course and time-distance relationships for surround suppression in macaque V1 neurons. *Journal of Neuroscience, 23*(20), 7690-7701.

Barcelo, F., Suwazono, S., & Knight, R. T. (2000). Prefrontal modulation of visual processing in humans. *Nature Neuroscience, 3*(4), 399.

Bastos, A. M., Vezoli, J., Bosman, C. A., Schoffelen, J. M., Oostenveld, R., Dowdall, J. R., ... & Fries, P. (2015). Visual areas exert feedforward and feedback influences through distinct frequency channels. *Neuron, 85*(2), 390-401.

Bosman, C. A., Schoffelen, J. M., Brunet, N., Oostenveld, R., Bastos, A. M., Womelsdorf, T., ... & Fries, P. (2012). Attentional stimulus selection through

selective synchronization between monkey visual areas. *Neuron, 75*(5), 875-888.

Buffalo, E. A., Fries, P., Landman, R., Liang, H., & Desimone, R. (2010). A backward progression of attentional effects in the ventral stream. *Proceedings of the National Academy of Sciences, 107*(1), 361-365.

Buschman, T. J., & Kastner, S. (2015). From behavior to neural dynamics: an integrated theory of attention. *Neuron, 88*(1), 127-144.

Buzsáki, G., Anastassiou, C. A., & Koch, C. (2012). The origin of extracellular fields and currents—EEG, ECoG, LFP and spikes. *Nature Reviews Neuroscience, 13*(6), 407.

Canolty, R. T., Soltani, M., Dalal, S. S., Edwards, E., Dronkers, N. F., Nagarajan, S. S., ... & Knight, R. T. (2007). Spatiotemporal dynamics of word processing in the human brain. *Frontiers in Neuroscience, 1*, 14.

Caspari, N., Janssens, T., Mantini, D., Vandenberghe, R., & Vanduffel, W. (2015). Covert shifts of spatial attention in the macaque monkey. *Journal of Neuroscience, 35*(20), 7695-7714.

Chalk, M., Herrero, J. L., Gieselmann, M. A., Delicato, L. S., Gotthardt, S., & Thiele, A. (2010). Attention reduces stimulus-driven gamma frequency oscillations and spike field coherence in V1. *Neuron, 66*(1), 114-125.

Cheung, C., Hamilton, L. S., Johnson, K., & Chang, E. F. (2016). The auditory representation of speech sounds in human motor cortex. *Elife, 5*, e12577.

Cook, E. P., & Maunsell, J. H. (2002). Attentional modulation of behavioral performance and neuronal responses in middle temporal and ventral intraparietal areas of macaque monkey. *Journal of Neuroscience, 22*(5), 1994-2004.

Corbetta, M., & Shulman, G. L. (2002). Control of goal-directed and stimulus-driven

attention in the brain. *Nature Reviews Neuroscience, 3*(3), 201.

Corbetta, M., & Shulman, G. L. (2011). Spatial neglect and attention networks. *Annual Review of Neuroscience, 34*, 569-599.

Cox, M. A., Dougherty, K., Adams, G. K., Reavis, E. A., Westerberg, J. A., Moore, B. S., ... & Maier, A. (2017). Spiking suppression precedes cued attentional enhancement of neural responses in primary visual cortex. *Cerebral Cortex*, 1-14.

Crone, N. E., Miglioretti, D. L., Gordon, B., & Lesser, R. P. (1998). Functional mapping of human sensorimotor cortex with electrocorticographic spectral analysis. II. Event-related synchronization in the gamma band. *Brain: A Journal of Neurology, 121*(12), 2301-2315.

Crone, N. E., Sinai, A., & Korzeniewska, A. (2006). High-frequency gamma oscillations and human brain mapping with electrocorticography. *Progress in Brain Research, 159*, 275-295.

Crone, N. E., Korzeniewska, A., & Franaszczuk, P. J. (2011). Cortical gamma responses: searching high and low. *International Journal of Psychophysiology, 79*(1), 9-15.

Daitch, A. L., Foster, B. L., Schrouff, J., Rangarajan, V., Kaşikçi, I., Gattas, S., & Parvizi, J. (2016). Mapping human temporal and parietal neuronal population activity and functional coupling during mathematical cognition. *Proceedings of the National Academy of Sciences, 113*(46), E7277-E7286.

Dale, A. M., Fischl, B., & Sereno, M. I. (1999). Cortical surface-based analysis: I. segmentation and surface reconstruction. *Neuroimage, 9*(2), 179-194.

Davidesco, I., Harel, M., Ramot, M., Kramer, U., Kipervasser, S., Andelman, F., ... &

1161 Malach, R. (2013). Spatial and object-based attention modulates broadband high-
1162 frequency responses across the human visual cortical hierarchy. *Journal of*
1163 *Neuroscience, 33*(3), 1228-1240.
1164 Delorme, A., & Makeig, S. (2004). EEGLAB: an open source toolbox for analysis of
1165 single-trial EEG dynamics including independent component analysis. *Journal of*
1166 *Neuroscience Methods, 134*(1), 9-21.
1167 Desikan, R. S., Ségonne, F., Fischl, B., Quinn, B. T., Dickerson, B. C., Blacker, D., ... &
1168 Albert, M. S. (2006). An automated labeling system for subdividing the human
1169 cerebral cortex on MRI scans into gyral based regions of interest. *Neuroimage,*
1170 *31*(3), 968-980.
1171 Desimone, R., & Duncan, J. (1995). Neural mechanisms of selective visual attention.
1172 *Annual Review of Neuroscience, 18*(1), 193-222.
1173 Di Russo, F., Martínez, A., & Hillyard, S. A. (2003). Source analysis of event-related
1174 cortical activity during visuo-spatial attention. *Cerebral Cortex, 13*(5), 486-499.
1175 Dumoulin, S. O., & Wandell, B. A. (2008). Population receptive field estimates in human
1176 visual cortex. *Neuroimage, 39*(2), 647-660.
1177 Engel, A. K., & Fries, P. (2010). Beta-band oscillations—signalling the status quo?
1178 *Current Opinion in Neurobiology, 20*(2), 156-165.
1179 Eriksen, B. A., & Eriksen, C. W. (1974). Effects of noise letters upon the identification of
1180 a target letter in a nonsearch task. *Perception & Psychophysics, 16*(1), 143-149.
1181 Eriksen, C. W. (1995). The flankers task and response competition: A useful tool for
1182 investigating a variety of cognitive problems. *Visual Cognition, 2*(2-3), 101-118.
1183 Felleman, D. J., & Van Essen, D. C. (1987). Receptive field properties of neurons in

1184 area V3 of macaque monkey extrastriate cortex. *Journal of Neurophysiology, 57*(4),
1185 889-920.
1186 Felleman, D. J., & Van Essen, D. C. (1991). Distributed hierarchical processing in the
1187 primate cerebral cortex. *Cerebral Cortex, 1*(1), 1-47.
1188 Fischl, B., Sereno, M. I., & Dale, A. M. (1999). Cortical surface-based analysis: II:
1189 inflation, flattening, and a surface-based coordinate system. *Neuroimage, 9*(2),
1190 195-207.
1191 Flinker, A., Chang, E. F., Barbaro, N. M., Berger, M. S., & Knight, R. T. (2011). Sub-
1192 centimeter language organization in the human temporal lobe. *Brain and*
1193 *Language, 117*(3), 103-109.
1194 Freud, E., Plaut, D. C., & Behrmann, M. (2016). 'What' is happening in the dorsal visual
1195 pathway. *Trends in Cognitive Sciences, 20*(10), 773-784.
1196 Fries, P. (2009). Neuronal gamma-band synchronization as a fundamental process in
1197 cortical computation. *Annual Review of Neuroscience, 32*, 209-224.
1198 Golumbic, E. M. Z., Ding, N., Bickel, S., Lakatos, P., Schevon, C. A., McKhann, G. M.,
1199 ... & Poeppel, D. (2013). Mechanisms underlying selective neuronal tracking of
1200 attended speech at a "cocktail party". *Neuron, 77*(5), 980-991.
1201 Gregoriou, G. G., Gotts, S. J., Zhou, H., & Desimone, R. (2009). High-frequency, long-
1202 range coupling between prefrontal and visual cortex during attention. *Science,*
1203 *324*(5931), 1207-1210.
1204 Grunewald, A., Bradley, D. C., & Andersen, R. A. (2002). Neural correlates of structure-
1205 from-motion perception in macaque V1 and MT. *Journal of Neuroscience, 22*(14),
1206 6195-6207.

1207 Halassa, M. M., & Kastner, S. (2017). Thalamic functions in distributed cognitive control.
1208 *Nature Neuroscience, 20*(12), 1669-1679.
1209 Hermes, D., Miller, K. J., Vansteensel, M. J., Aarnoutse, E. J., Leijten, F. S., & Ramsey,
1210 N. F. (2012). Neurophysiologic correlates of fMRI in human motor cortex. *Human*
1211 *Brain Mapping, 33*(7), 1689-1699.
1212 Ito, M., & Gilbert, C. D. (1999). Attention modulates contextual influences in the primary
1213 visual cortex of alert monkeys. *Neuron, 22*(3), 593-604.
1214 Kastner, S., & Ungerleider, L. G. (2000). Mechanisms of visual attention in the human
1215 cortex. *Annual Review of Neuroscience, 23*(1), 315-341.
1216 Kastner, S., Chen, Q., Jeong, S. K., & Mruczek, R. E. B. (2017). A brief comparative
1217 review of primate posterior parietal cortex: A novel hypothesis on the human
1218 toolmaker. *Neuropsychologia, 105*, 123-134.
1219 Kelly, S. P., Gomez-Ramirez, M., & Foxe, J. J. (2008). Spatial attention modulates initial
1220 afferent activity in human primary visual cortex. *Cerebral Cortex, 18*(11), 2629-
1221 2636.
1222 Klein, B. P., Harvey, B. M., & Dumoulin, S. O. (2014). Attraction of position preference
1223 by spatial attention throughout human visual cortex. *Neuron, 84*(1), 227-237.
1224 Konen, C. S., & Kastner, S. (2008). Representation of eye movements and stimulus
1225 motion in topographically organized areas of human posterior parietal cortex.
1226 *Journal of Neuroscience, 28*(33), 8361-8375.
1227 Konen, C. S., Mruczek, R. E., Montoya, J. L., & Kastner, S. (2013). Functional
1228 organization of human posterior parietal cortex: grasping-and reaching-related
1229 activations relative to topographically organized cortex. *Journal of Neurophysiology,*

109(12), 2897-2908.

Kreiman, G., Hung, C. P., Kraskov, A., Quiroga, R. Q., Poggio, T., & DiCarlo, J. J. (2006). Object selectivity of local field potentials and spikes in the macaque inferior temporal cortex. *Neuron, 49*(3), 433-445.

Lachaux, J. P., George, N., Tallon-Baudry, C., Martinerie, J., Hugueville, L., Minotti, L., ... & Renault, B. (2005). The many faces of the gamma band response to complex visual stimuli. *Neuroimage, 25*(2), 491-501.

Lee, J., Williford, T., & Maunsell, J. H. (2007). Spatial attention and the latency of neuronal responses in macaque area V4. *Journal of Neuroscience, 27*(36), 9632-9637.

Lehky, S. R., & Sereno, A. B. (2007). Comparison of shape encoding in primate dorsal and ventral visual pathways. *Journal of Neurophysiology, 97*(1), 307-319.

Leszczyński, M., Barczak, A., Kajikawa, Y., Ulbert, I., Tal, I., Falchier, A. Y., Haegens, S., Knight, R. T., & Schroeder, C. E. (2018). Dissociation of broadband high-frequency activity and neuronal firing in the primary sensory cortices. (submitted for publication).

Lisman, J. E., & Jensen, O. (2013). The theta-gamma neural code. *Neuron, 77*(6), 1002-1016.

Luck, S. J., Girelli, M., McDermott, M. T., & Ford, M. A. (1997). Bridging the gap between monkey neurophysiology and human perception: An ambiguity resolution theory of visual selective attention. *Cognitive Psychology, 33*(1), 64-87.

Marcus, D. S., & Van Essen, D. C. (2002). Scene segmentation and attention in primate cortical areas V1 and V2. *Journal of Neurophysiology, 88*(5), 2648-2658.

1253 Maris, E., & Oostenveld, R. (2007). Nonparametric statistical testing of EEG-and MEG-
1254 data. *Journal of Neuroscience Methods, 164*(1), 177-190.
1255 Markov, N. T., Vezoli, J., Chameau, P., Falchier, A., Quilodran, R., Huissoud, C., ... &
1256 Barone, P. (2014). Anatomy of hierarchy: feedforward and feedback pathways in
1257 macaque visual cortex. *Journal of Comparative Neurology, 522*(1), 225-259.
1258 Martinez, A., Anllo-Vento, L., Sereno, M. I., Frank, L. R., Buxton, R. B., Dubowitz, D. J.,
1259 ... & Hillyard, S. A. (1999). Involvement of striate and extrastriate visual cortical
1260 areas in spatial attention. *Nature Neuroscience, 2*(4), 364-369.
1261 McAdams, C. J., & Maunsell, J. H. (1999). Effects of attention on the reliability of
1262 individual neurons in monkey visual cortex. *Neuron, 23*(4), 765-773.
1263 McAlonan, K., Cavanaugh, J., & Wurtz, R. H. (2008). Guarding the gateway to cortex
1264 with attention in visual thalamus. *Nature, 456*(7220), 391-394.
1265 Mehta, A. D., Ulbert, I., & Schroeder, C. E. (2000). Intermodal selective attention in
1266 monkeys. I: distribution and timing of effects across visual areas. *Cerebral Cortex,*
1267 *10*(4), 343-358.
1268 Mesgarani, N., Cheung, C., Johnson, K., & Chang, E. F. (2014). Phonetic feature
1269 encoding in human superior temporal gyrus. *Science, 343*(6174), 1006-1010.
1270 Michalareas, G., Vezoli, J., Van Pelt, S., Schoffelen, J. M., Kennedy, H., & Fries, P.
1271 (2016). Alpha-beta and gamma rhythms subserve feedback and feedforward
1272 influences among human visual cortical areas. *Neuron, 89*(2), 384-397.
1273 Moore, T., & Armstrong, K. M. (2003). Selective gating of visual signals by
1274 microstimulation of frontal cortex. *Nature, 421*(6921), 370-373.
1275 Moore, T., & Zirnsak, M. (2017). Neural mechanisms of selective visual attention.

Annual Review of Psychology, 68, 47-72.

Motter, B. C. (1993). Focal attention produces spatially selective processing in visual cortical areas V1, V2, and V4 in the presence of competing stimuli. *Journal of Neurophysiology, 70*(3), 909-919.

Mruczek, R. E., von Loga, I. S., & Kastner, S. (2013). The representation of tool and non-tool object information in the human intraparietal sulcus. *Journal of Neurophysiology, 109*(12), 2883-2896.

O'Connor, D. H., Fukui, M. M., Pinsk, M. A., & Kastner, S. (2002). Attention modulates responses in the human lateral geniculate nucleus. *Nature Neuroscience, 5*(11), 1203-1209.

Ozeki, H., Finn, I. M., Schaffer, E. S., Miller, K. D., & Ferster, D. (2009). Inhibitory stabilization of the cortical network underlies visual surround suppression. *Neuron, 62*(4), 578-592.

Parvizi, J., Jacques, C., Foster, B. L., Withoft, N., Rangarajan, V., Weiner, K. S., & Grill-Spector, K. (2012). Electrical stimulation of human fusiform face-selective regions distorts face perception. *Journal of Neuroscience, 32*(43), 14915-14920.

Parvizi, J., & Kastner, S. (2018). Promises and limitations of human intracranial electroencephalography. *Nature Neuroscience, 21*, 474-483.

Raiguel, S. E., Lagae, L., Gulyàs, B., & Orban, G. A. (1989). Response latencies of visual cells in macaque areas V1, V2 and V5. *Brain Research, 493*(1), 155-159.

Ray, S., Crone, N. E., Niebur, E., Franaszczuk, P. J., & Hsiao, S. S. (2008a). Neural correlates of high-gamma oscillations (60–200 Hz) in macaque local field potentials and their potential implications in electrocorticography. *Journal of Neuroscience,*

28(45), 11526-11536.

Ray, S., Niebur, E., Hsiao, S. S., Sinai, A., & Crone, N. E. (2008b). High-frequency gamma activity (80–150 Hz) is increased in human cortex during selective attention. *Clinical Neurophysiology, 119*(1), 116-133.

Ray, S., & Maunsell, J. H. (2011). Different origins of gamma rhythm and high-gamma activity in macaque visual cortex. *PLoS Biology, 9*(4), e1000610.

Reynolds, J. H., & Chelazzi, L. (2004). Attentional modulation of visual processing. *Annual Review of Neuroscience, 27*, 611-647.

Rich, E. L., & Wallis, J. D. (2017). Spatiotemporal dynamics of information encoding revealed in orbitofrontal high-gamma. *Nature Communications, 8*(1), 1139.

Saad, Z. S., Reynolds, R. C., Argall, B., Japee, S., & Cox, R. W. (2004). SUMA: an interface for surface-based intra-and inter-subject analysis with AFNI. *IEEE International Symposium on Biomedical Imaging: Nano to Macro,* 1510-1513.

Saalmann, Y. B., & Kastner, S. (2011). Cognitive and perceptual functions of the visual thalamus. *Neuron, 71*(2), 209-223.

Saalmann, Y. B., Pinsk, M. A., Wang, L., Li, X., & Kastner, S. (2012). The pulvinar regulates information transmission between cortical areas based on attention demands. *Science, 337*(6095), 753-756.

Schmolesky, M. T., Wang, Y., Hanes, D. P., Thompson, K. G., Leutgeb, S., Schall, J. D., & Leventhal, A. G. (1998). Signal timing across the macaque visual system. *Journal of Neurophysiology, 79*(6), 3272-3278.

Siegel, M., Donner, T. H., Oostenveld, R., Fries, P., & Engel, A. K. (2008). Neuronal synchronization along the dorsal visual pathway reflects the focus of spatial

1322 attention. *Neuron, 60*(4), 709-719.
1323 Silver, M. A., & Kastner, S. (2009). Topographic maps in human frontal and parietal
1324 cortex. *Trends in Cognitive Sciences, 13*(11), 488-495.
1325 Sundberg, K. A., Mitchell, J. F., Gawne, T. J., & Reynolds, J. H. (2012). Attention
1326 influences single unit and local field potential response latencies in visual cortical
1327 area V4. *Journal of Neuroscience, 32*(45), 16040-16050.
1328 Szczepanski, S. M., Konen, C. S., & Kastner, S. (2010). Mechanisms of spatial attention
1329 control in frontal and parietal cortex. *Journal of Neuroscience, 30*(1), 148-160.
1330 Szczepanski, S. M., Pinsk, M. A., Douglas, M. M., Kastner, S., & Saalmann, Y. B.
1331 (2013). Functional and structural architecture of the human dorsal frontoparietal
1332 attention network. *Proceedings of the National Academy of Sciences, 110*(39),
1333 15806-15811.
1334 Szczepanski, S. M., Crone, N. E., Kuperman, R. A., Auguste, K. I., Parvizi, J., & Knight,
1335 R. T. (2014). Dynamic changes in phase-amplitude coupling facilitate spatial
1336 attention control in fronto-parietal cortex. *PLoS Biology, 12*(8), e1001936.
1337 Van Kerkoerle, T., Self, M. W., Dagnino, B., Gariel-Mathis, M. A., Poort, J., Van Der
1338 Togt, C., & Roelfsema, P. R. (2014). Alpha and gamma oscillations characterize
1339 feedback and feedforward processing in monkey visual cortex. *Proceedings of the*
1340 *National Academy of Sciences, 111*(40), 14332-14341.
1341 Voytek, B., D'esposito, M., Crone, N., & Knight, R. T. (2013). A method for event-related
1342 phase/amplitude coupling. *Neuroimage, 64*, 416-424.
1343 Wandell, B. A., & Winawer, J. (2015). Computational neuroimaging and population
1344 receptive fields. *Trends in Cognitive Sciences, 19*(6), 349-357.

1345 Wang, L., Mruczek, R. E., Arcaro, M. J., & Kastner, S. (2015). Probabilistic maps of
1346 visual topography in human cortex. *Cerebral Cortex, 25*(10), 3911-3931.
1347 Watson, B. O., Ding, M., & Buzsáki, G. (2018). Temporal coupling of field potentials and
1348 action potentials in the neocortex. *European Journal of Neuroscience,* 1-16.
1349 Wimmer, R. D., Schmitt, L. I., Davidson, T. J., Nakajima, M., Deisseroth, K., & Halassa,
1350 M. M. (2015). Thalamic control of sensory selection in divided attention. *Nature,*
1351 *526*(7575), 705-709.
1352 Winawer, J., & Parvizi, J. (2016). Linking electrical stimulation of human primary visual
1353 cortex, size of affected cortical area, neuronal responses, and subjective
1354 experience. *Neuron, 92*(6), 1213-1219.
1355 Womelsdorf, T., Anton-Erxleben, K., Pieper, F., & Treue, S. (2006). Dynamic shifts of
1356 visual receptive fields in cortical area MT by spatial attention. *Nature Neuroscience,*
1357 *9*(9), 1156-1160.
1358 Yoshor, D., Ghose, G. M., Bosking, W. H., Sun, P., & Maunsell, J. H. (2007). Spatial
1359 attention does not strongly modulate neuronal responses in early human visual
1360 cortex. *Journal of Neuroscience, 27*(48), 13205-13209.
1361 Zhang, S., Xu, M., Kamigaki, T., Do, J. P. H., Chang, W. C., Jenvay, S., ... & Dan, Y.
1362 (2014). Long-range and local circuits for top-down modulation of visual cortex
1363 processing. *Science, 345*(6197), 660-665.
1364

Figure and Table Legends

Figure 1. Electrode coverage. Electrode locations (combined across 8 patients; N = 636) rendered onto a brain surface in standardized space, shown from posterior, lateral, and medial views. A probabilistic atlas of visuospatial topographic areas (Wang et al., 2015) is superimposed to clarify electrode locations relative to retinotopically organized cortex (see color-code for areas to the right). Individual subject's electrodes were localized on their brain surfaces after aligning post-operative CT images of the implanted electrodes with pre-operative structural MRIs; the surfaces and electrode locations were converted to a standard surface template. The probabilistic atlas was superimposed, and electrodes that overlapped the atlas maximum probability map were assigned to the maximally probable area (see Methods for further details).

Figure 2. Task and example responses. A: Subjects performed a variant of the Eriksen flanker task. After maintaining central fixation for 1100 ms, a brief cue indicated the location of a target shape, which was displayed in a circular array after a variable delay of 300-700 ms. Targets were either barrel or bow tie shapes, and flanking stimuli were either congruent (same shape) or incongruent (different shape). Subjects responded to indicate the target shape using a left or right mouse-button press. **B:** Intracranial field potential (IFP) power recorded from one electrode located in area V3d as a function of frequency during baseline (black line; 200 ms before cue onset) and visually-evoked (orange line; 50-250 ms after cue onset) windows, mean ± sem across trials (N = 149). **C:** Relative cue-evoked IFP power (d' of baseline), mean across trials at the location exerting the strongest HFB response (same electrode as in B). Time 0

denotes cue onset. Colorscale: ±2.5. **D:** Mean cue-evoked HFB power (70-200 Hz, d' of baseline) at each cue location on a trial-by-trial basis (same electrode as in B and C). Trials were sorted as a function of distance from the location exerting the strongest HFB response (response field center, RF_C). Colorscale: ±30. Top panel, mean normalized power over time at RF_C ± trial-wise sem. Right panel, mean normalized cue-evoked power at each cue location ± trial-wise sem.

Figure 3. Spatial specificity of task-related HFB response fields. Recordings from four adjacent electrodes in subject S3 (10 mm strip spacing). **A:** Electrode positions projected on the subject's anatomical MRI surface in relation to the probabilistic atlas (color-coded atlas legend as in Figure 1). Electrode diameters are shown to scale. Blank circles indicate electrodes in the strip lacking response fields. **B-E:** IFP power spectra (mean across trials) evoked by the cue (left panels) and array (right panels) at each of the 14 cue locations. Cue-evoked power is shown as d' of baseline power, indicating visually-evoked responses. Array-evoked power is shown as d' of power at RF_{null}, indicating the effect of spatial attention. Central panels: circular tuning curves showing normalized HFB power at each location evoked by the cue (mean of 50-250 ms after cue, solid orange line), during the delay (mean of 200 ms before array, dashed purple line), and in response to the array (mean of 300-500 ms after array onset, solid purple line). Polar grid lines indicate normalized minimum and maximum enhancement. Adjacent electrodes are shown from areas IPS0 (B, C), V3B (D), and V3d (E). Note the reversal in field location from lower to upper quadrant in adjacent electrodes, indicating the high spatial specificity of HFB responses.

Figure 4. Timecourses and response onset latencies of cue-evoked HFB responses. A: Mean, normalized HFB power at RF_C relative to cue onset, by topographic area for sites with response fields (same sites as in Figure 4). Color codes for areas are indicated in panel B. **B:** Mean response onset latency ± 95%CI by area. N indicates number of sites per area included in the analysis. **C:** Response onset latencies of sites with response fields by area. Number of sites per area is indicated in parentheses.

Figure 5. Examples of attentional modulation effects during the delay and in response to the array. Upper panels: Attentional enhancement during the delay and in response to the array. Mean responses ±95%CI evoked by the array during attend-to-RF_C (green) and attend-to-RF_{null} (gray) trials from an example TO electrode (left) and the TO population (right). **Middle panels:** Attentional suppression in response to the array for an example V1v electrode (left) and the V1 population (right). **Lower panels:** Mixed effects of attentional enhancement and suppression for an example IPS3 electrode showing attentional enhancement during the delay, but suppression in response to the array (left). In the IPS3 population response (right), only the elevated delay effect persists, whereas suppression and enhancement effects in individual electrodes cancel each other out to result in no modulatory net effect in response to the array. Vertical lines indicate attentional modulation latencies.

Figure 6. Topography of attentional modulation effects during the delay and in response to the array. Color indicates the modulation index (MI) for sites with a

response field across all subjects rendered onto a brain surface in standardized space, shown from posterior, lateral, and medial views. Large dots: topographic sites. Small dots: non-topographic sites. **A:** Topography and strength of attentional modulation during the delay (200 ms before array onset, only trials with delays longer than 450 ms were included in the analysis). **B**: Topography and strength of attentional modulation in response to the array in the late window (300-500 ms after array onset). Red colors: enhancement effects; green colors: suppression effects.

Figure 7. Strengths of attentional modulation during the delay and in response to the array. A: Attentional modulation index (MI) in each area during the delay (200 ms before array onset) using trials with delays longer than 450 ms. Mean modulation index (±95%CI) shown separately for enhancement and suppression effects obtained in each area at the population level. * indicates bootstrapped randomization test $p < 0.05$ compared to 0. Outlined bars shown for areas with a single electrode exhibiting the effect. **B:** As in A for modulation during the early array window (50-200 ms after array onset). **C:** As in A for modulation during the late array window (300-500 ms after array onset).

Figure 8. Timecourses of array-evoked HFB responses. Mean, normalized power (±95%CI) when attention was allocated at RF_C (colored by area) and RF_{null} (gray), aligned to array onset. Topographic areas with significant response enhancement effects are shown (population responses). Vertical lines indicate attentional modulation latencies.

Figure 9. Attentional modulation latencies. A: Mean modulation latency (±95%CI) by area. N indicates number of electrodes per area included in the analysis. **B:** Cumulative distributions of modulation latencies for each area. Color codes for areas are indicated in panel A.

Figure 10. Spatial tuning widths of cue-evoked HFB response fields. A: Spatial tuning curves of cue-evoked mean HFB responses relative to baseline, normalized and centered on RF_C and pooled across all sites with spatial response fields recorded within a given topographic area, ± 95%CI. Color codes for areas are indicated in panel B. **B:** Mean width of tuning curves ± 95%CI. N indicates number of sites per area included in the analysis. **C:** Tuning widths of sites with response fields by area. Number of sites per area is indicated in parentheses.

Figure 11. Cue-evoked response fields, memory, and attention fields. A: Mean field width of population tuning curves (±95%CI) for cue-evoked response fields versus memory fields for areas with a significant enhanced MI in both windows. **B:** Widths of cue-evoked response fields versus attention fields. **C:** Widths of memory versus attention fields. Color codes for areas are indicated in previous figures.

Table 1. Patient information. Area coverage by lobe: O, occipital; P, parietal; T, temporal; LF, lateral frontal; MF, medial frontal. The number of electrodes indicates those that were included in the analysis relative to all implanted electrodes (in parentheses). *, † denote subjects tested with cues presented at 8 or 16 locations, respectively. All other subjects had cues presented at 14 locations. RH = right hemisphere; LH = left hemisphere.

Table 2. Response onset and attentional modulation latencies by area. Numbers in the second column refer to the response onset latencies for each area (mean ± 95%CI). Numbers in the third column refer to the attentional modulation latencies with the suppression effects in the parentheses. **-** denotes areas without significant attentional modulation.

Table 3. Response onset latencies and attentional modulation latencies: Significance by area. Response onset latencies (lower triangle): Significance after the Holm-Bonferroni sequential correction for multiple comparisons at target alpha level $p < 0.05$. **+** indicates that the latency of the column area was faster than the row area, and vice versa for **-**. Attentional modulation latencies (upper triangle): Significance after Holm-Bonferroni sequential correction for multiple comparisons at target alpha level $p < 0.05$. ✱ indicates that the latency of the column area was faster than the row area, and vice versa for ·. Blank indicates no significant difference between areas.

Table 4. Attentional modulation during the delay and in response to the array: Significance by area. Delay period (lower triangle): Significance after Holm-Bonferroni sequential correction for multiple comparisons at target alpha level $p < 0.05$. **+** indicates that the MI of the column area was weaker than the row area, and vice versa for **-**. Array period (upper triangle): Modulation index for attentional enhancement in the late array window (300-500 ms after array onset); significance after Holm-Bonferroni sequential correction for multiple comparisons at target alpha level $p < 0.05$. ✱ indicates that the MI of the column area was weaker than the row area, and vice versa for **·**. Blank indicates no significant difference between areas.

Table 5. Spatial tuning widths: Significance by area. Significance after Holm-Bonferroni sequential correction for multiple comparisons at target alpha level $p < 0.05$. **+** indicates that the tuning width of the column area was sharper than the row area, **·** indicates that the tuning width of the column area was broader than the row area, blank indicates no significant difference between areas.

Table 1. Patient information.

Sub	Sex	Age	Handedness	Coverage	Brain Areas	# Elecs	Acc	RT (ms)	# Trials
S1	M	45	Right	RH	O, P, T	99 (112)	96%	802 ± 13	200
S2	M	22	Left	LH	O, P, T	110 (128)	95%	765 ± 13	300
S3	F	22	Right	LH	LF, O, P, MF	86 (100)	83%	888 ± 17	200
S4[†]	M	18	Right	LH	O, P, T	86 (94)	87%[†]	1024 ± 16[†]	200
S5*	M	42	Left	LH	LF, O, P, T	52 (74)	97%*	599 ± 5*	300
S6	M	51	Right	LH	LF, P, MF	89 (106)	96%	1130 ± 15	250
S7	M	23	Right	LH	LF, P, T	52 (52)	98%	794 ± 11	250
S8[†]	F	56	Right	LH	LF, T	62 (64)	91%[†]	955 ± 19[†]	150

Table 2. Response onset and attentional modulation latencies by area.

Brain Areas	Cue Response Latency (ms)	Attention Latency (ms) Enhanced (Suppressed)
V1d/v	64 ± 1	83 ± 9, 315 ± 33 (68 ± 7)
V2d/v	66 ± 3	295 ± 16
V3d/v	82 ± 7	233 ± 12
V3A	80 ± 2	246 ± 8
V3B	81 ± 2	268 ± 22
TO1-2	128 ± 6	129 ± 3
IPS0	106 ± 5	156 ± 18
IPS1-2	120 ± 10	119 ± 22
IPS3	143 ± 1	225 ± 11 (265 ± 142)
IPS4-5, SPL1	137 ± 5	-
FEF	62 ± 5	-
vExtrastriate	149 ± 5	172 ± 7
Parietal	100 ± 3	124 ± 7
Frontal	84 ± 5	-
Temporal	109 ± 5	223 ± 16

Table 3. Response onset latencies and attentional modulation latencies: Significance by area.

Response Onset Latencies \ Attentional Modulation Latencies	V1d/v	V1c1	V1c2	V2d/v	V3d/v	V3A	V3B	TO	IPS0	IPS1-2	IPS3	IPS4+	FEF	LO/VO	Parietal	Frontal	Temporal
V1d/v																	
V1c1			·	·	·	·	·	·	·		·			·	·		·
V1c2					*	*	*	*	*	*	*			*	*		*
V2d/v								*	*	*				*	*		*
V3d/v	+			+				*	*	*				*	*		
V3A	+			+				*	*	*				*	*		
V3B	+			+				*	*	*				*	*		*
TO	+			+	+	+	+				·						
IPS0	+			+	+	+	+	-		*	·						·
IPS1-2	+			+	+	+	+		+		·						·
IPS3	+			+	+	+	+	+	+					*	*		
IPS4+	+			+	+	+	+	+	+	+							
FEF					-	-	-	-	-	-	-	-					
LO/VO	+			+	+	+	+	+	+	+			+				
Parietal				+						-	-	-	+	-			
Frontal				+				-		-	-	-	+	-			
Temporal	+			+	+					-	-	-	+	-	+	+	

Table 4. Attentional modulation during the delay and in response to the array: Significance by area.

Attentional Modulation Strength (Delay)	Attentional Modulation Strength (Array)													
	V1d/v	V2d/v	V3d/v	V3A	V3B	TO	IPS0	IPS1-2	IPS3	IPS4+	LO/VO	Parietal	Frontal	Temporal
V1d/v		·	·		·	·	·				·	·	·	·
V2d/v				*		·	·		*	*	·	·		·
V3d/v		+		*		·	·		*	*	·	·		·
V3A	+				·	·	·	·			·	·	·	·
V3B				-		·	·		*	*	·	·	*	·
TO	+	+	+	+	+		·	*	*	*		*	*	
IPS0	+	+	+	+	+			*	*	*	*	*	*	*
IPS1-2	+	+	+	+	+						·			
IPS3	+	+	+	+	+						·	·	·	·
IPS4+						-	-	-	-		·	·	·	·
LO/VO	+	+	+		+	-		-		+		*	*	*
Parietal	+	+	+	+	+		+		+	+	+		*	·
Frontal	+	+	+		+					+	+			·
Temporal	+	+	+	+	+					+	+			

Table 5. Spatial tuning widths: Significance by area.

	V1d/v	V2d/v	V3d/v	V3A	V3B	TO	IPS0	IPS1-2	IPS3	IPS4+	FEF	LO/VO	Parietal	Frontal	Temporal
V1d/v				•	•	•	•		•			•	•		•
V2d/v				•	•	•	•		•			•	•		•
V3d/v				•	•	•	•		•			•	•		•
V3A	+	+	+		•		•						•		
V3B	+	+	+	+			•						•		
TO	+	+	+								+			+	
IPS0	+	+	+	+	+							+	+	+	+
IPS1-2									•						
IPS3	+	+	+					+			+	+		+	+
IPS4+															
FEF						•			•					+	
LO/VO	+	+	+				•		•						
Parietal	+	+	+	+	+		•								
Frontal						•	•		•		•				
Temporal	+	+	+				•		•						

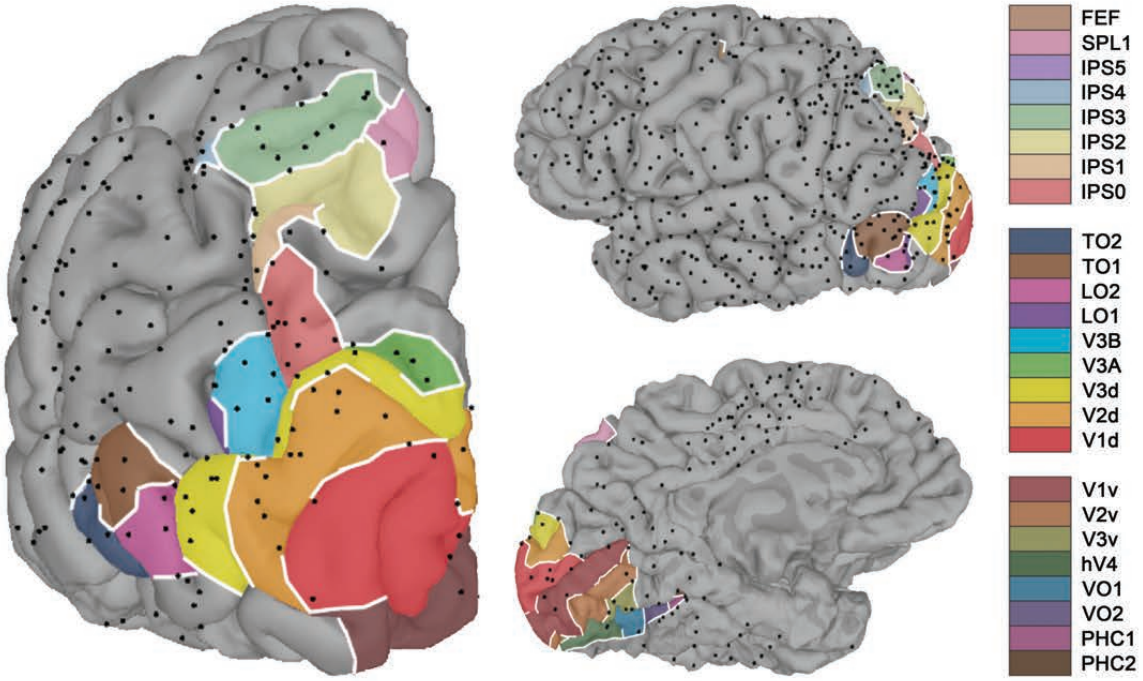

Figure 1

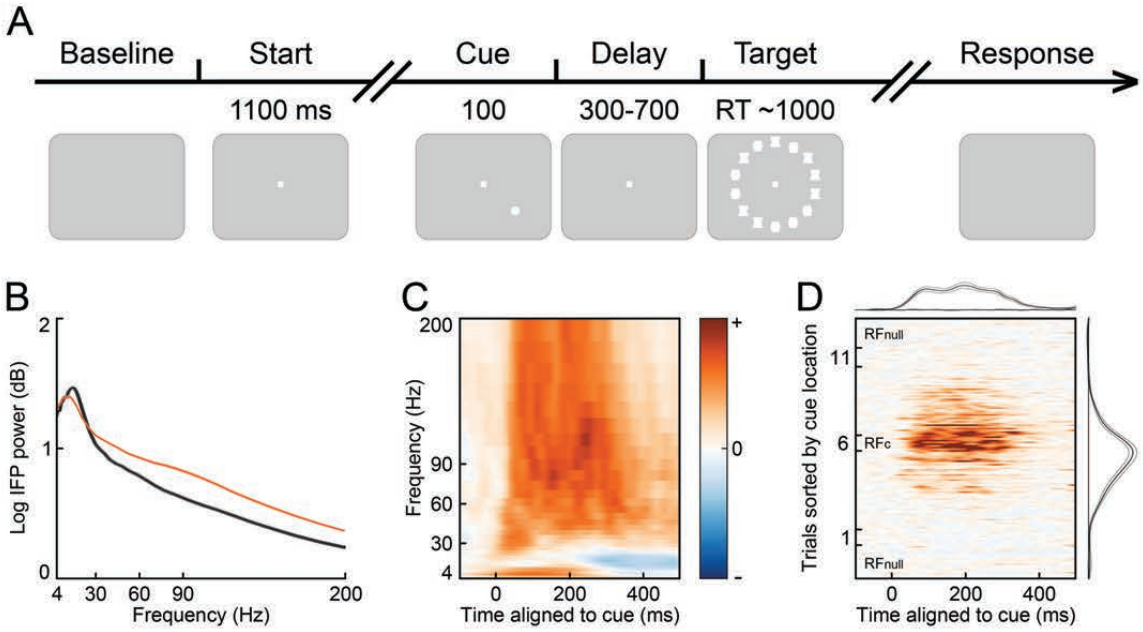

Figure 2

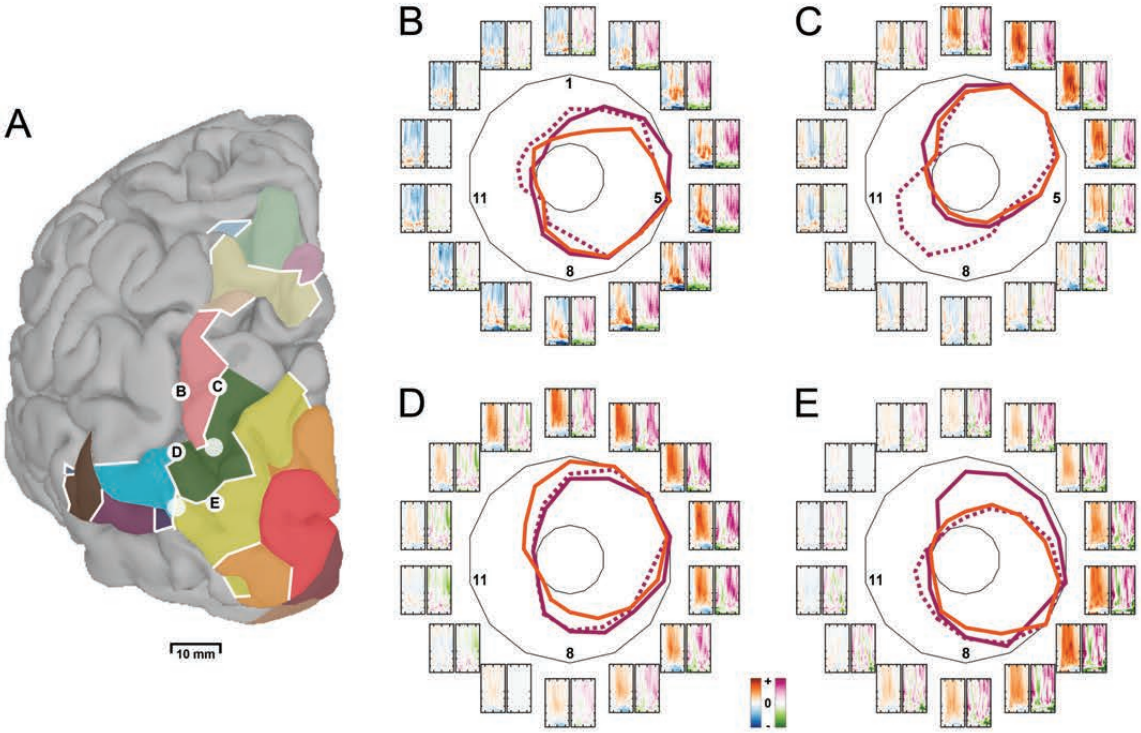

Figure 3

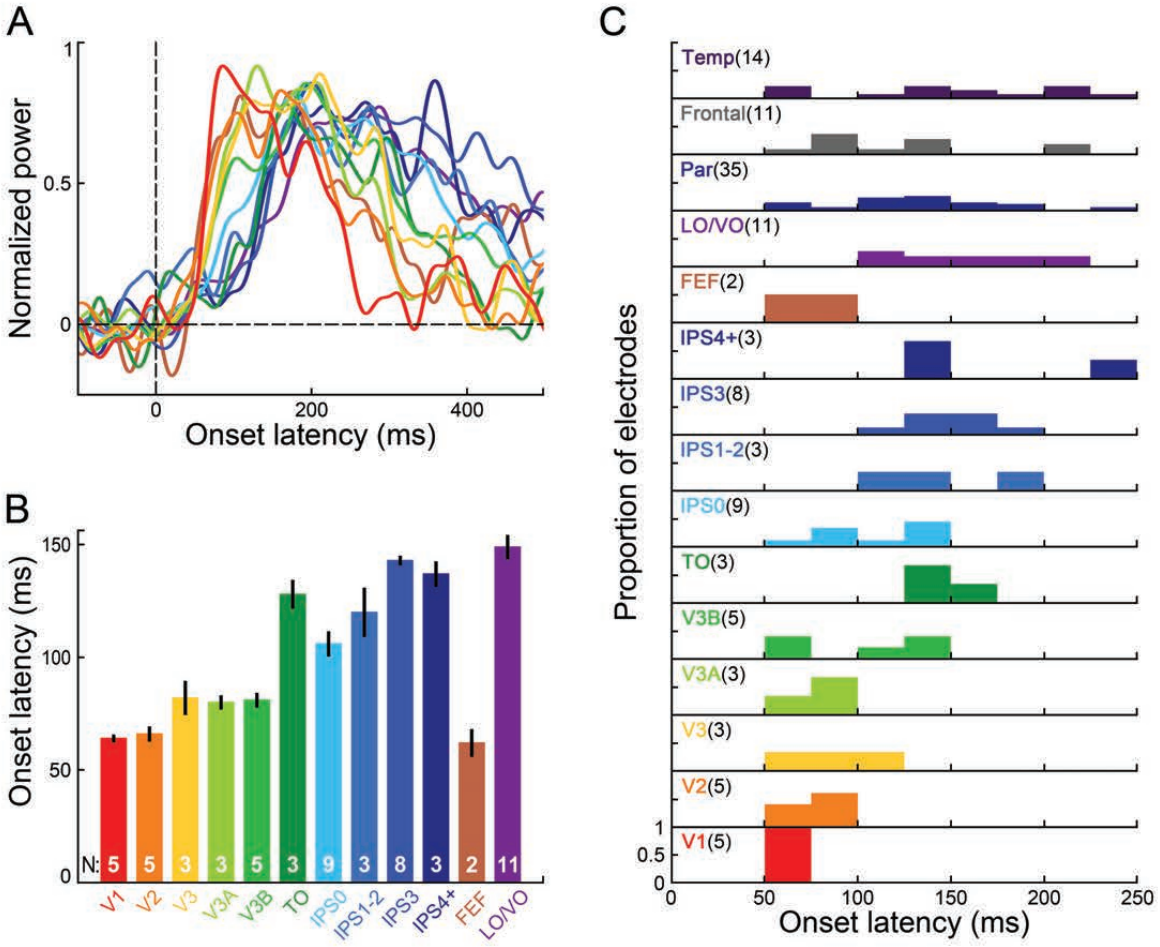

Figure 4

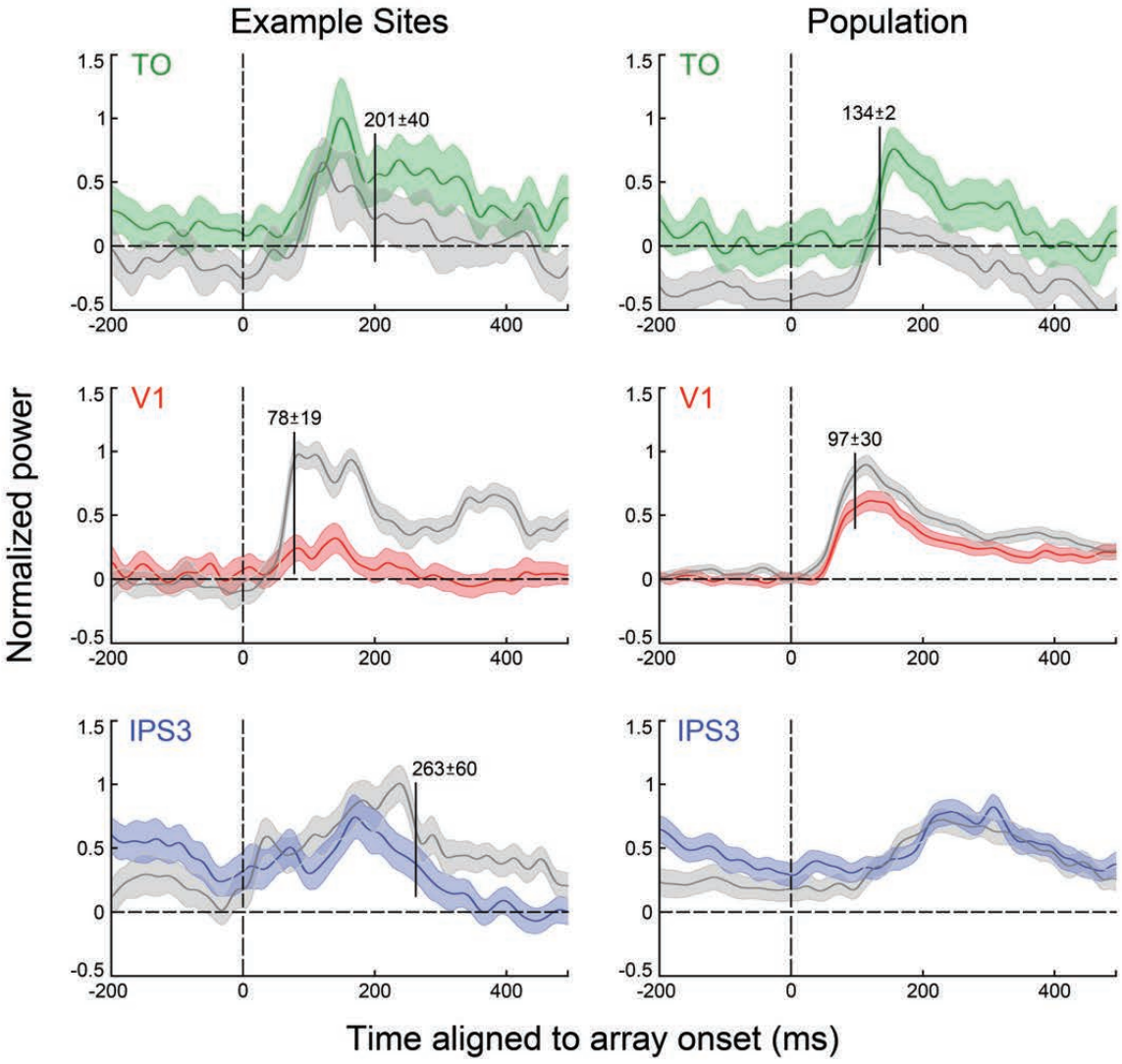

Figure 5

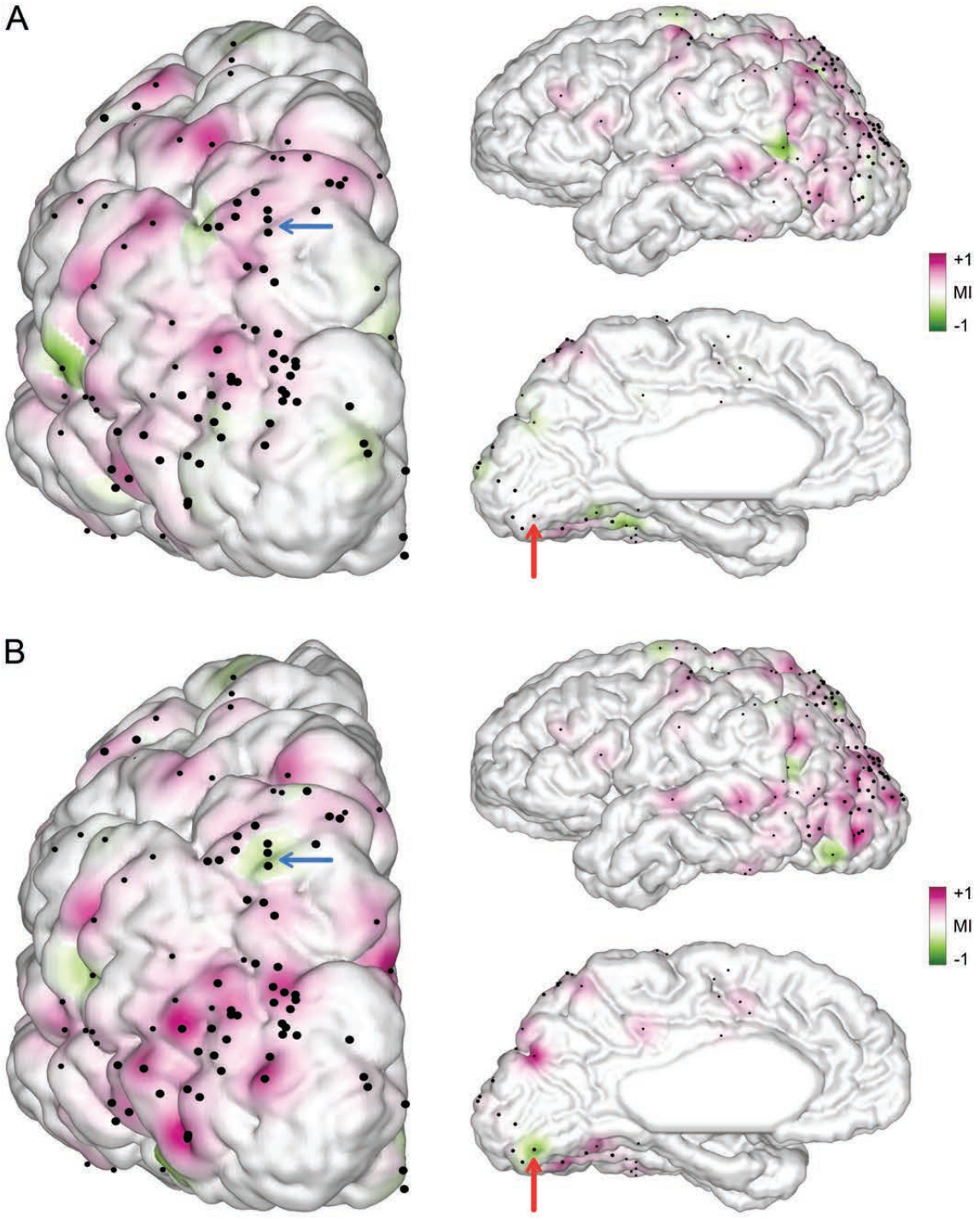

Figure 6

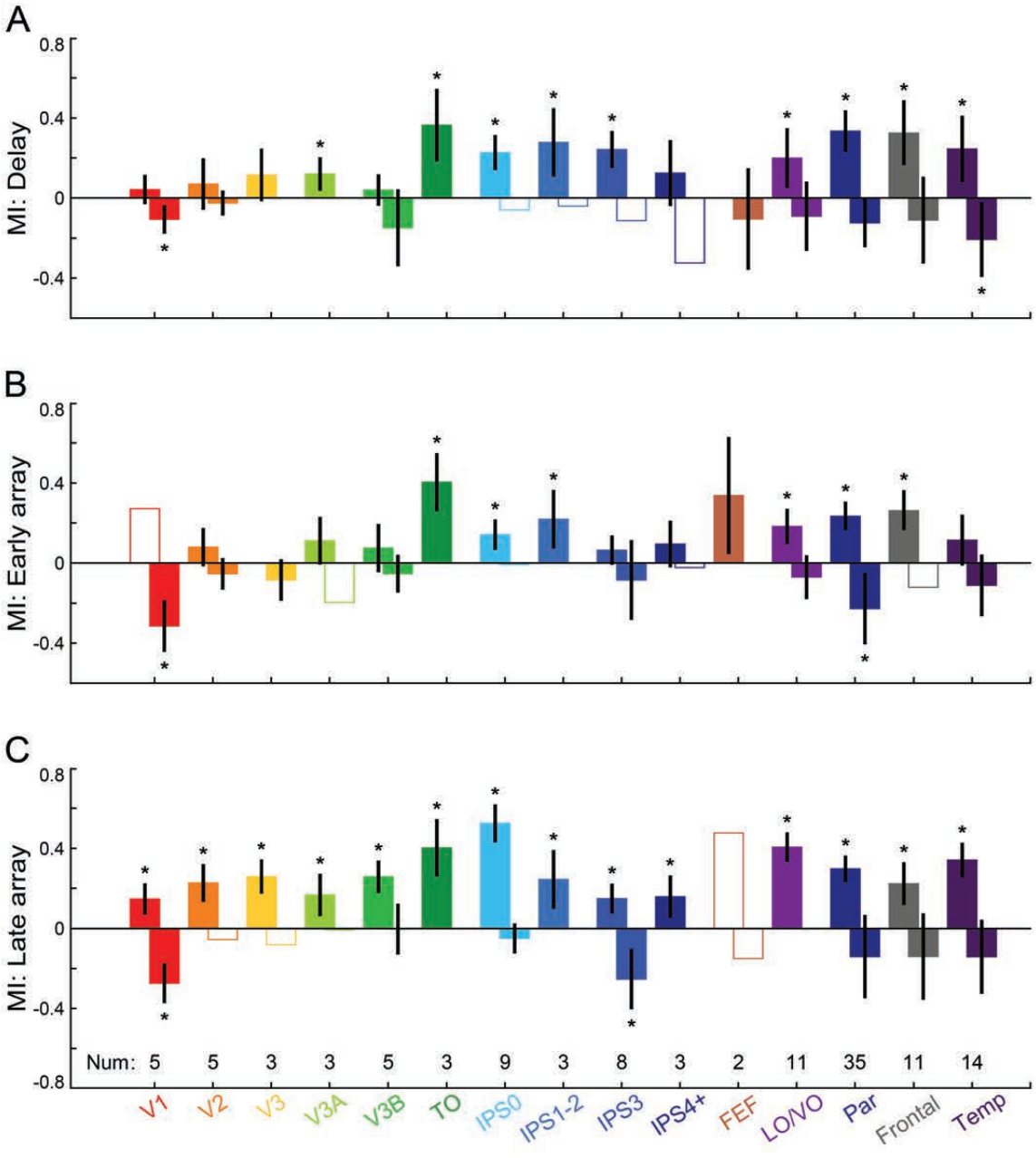

Figure 7

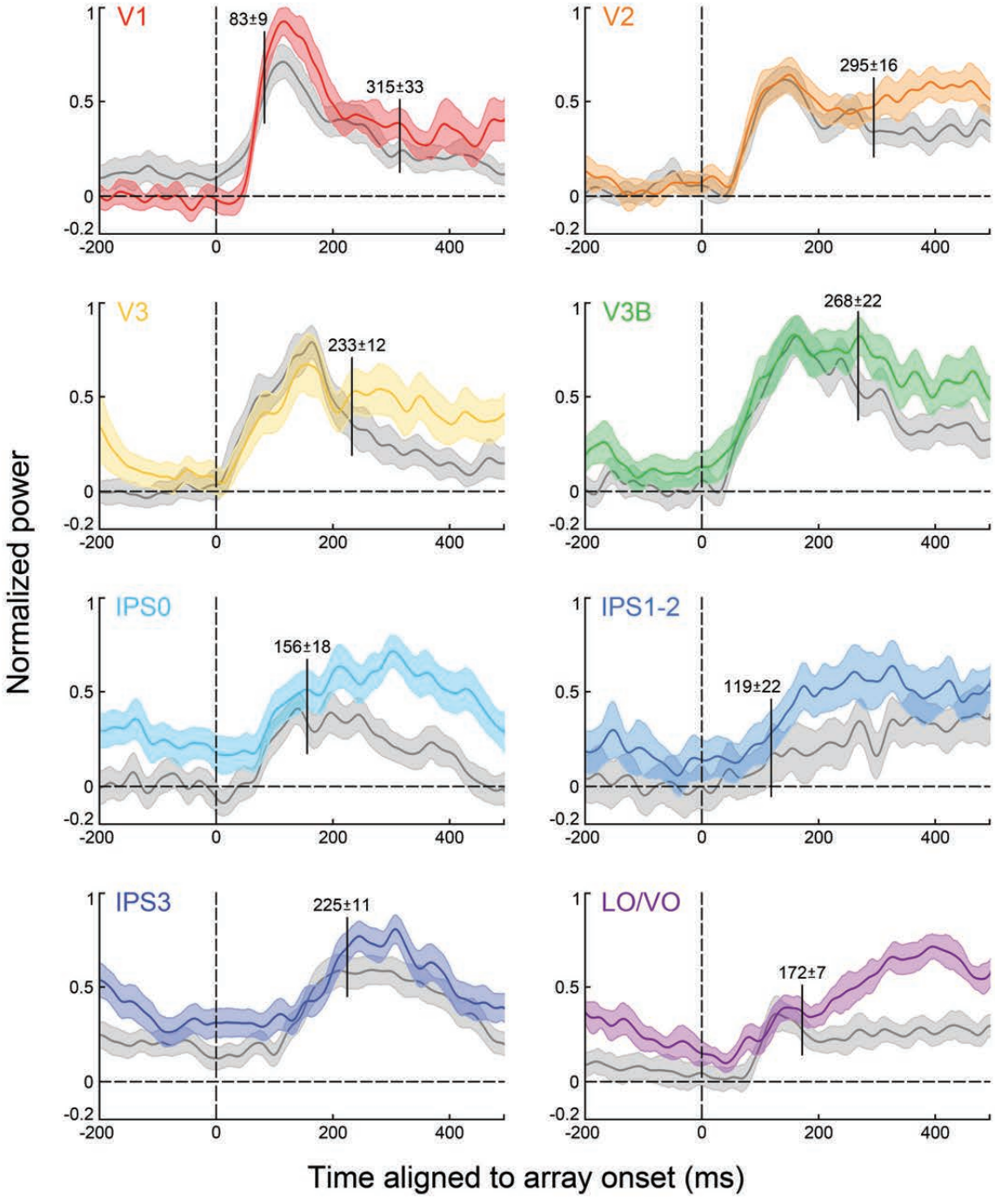

Figure 8

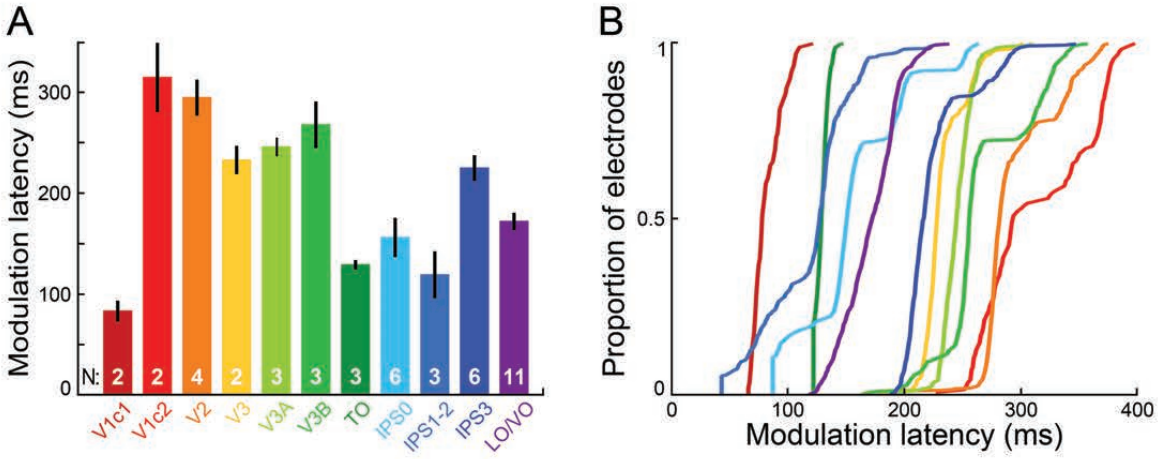

Figure 9

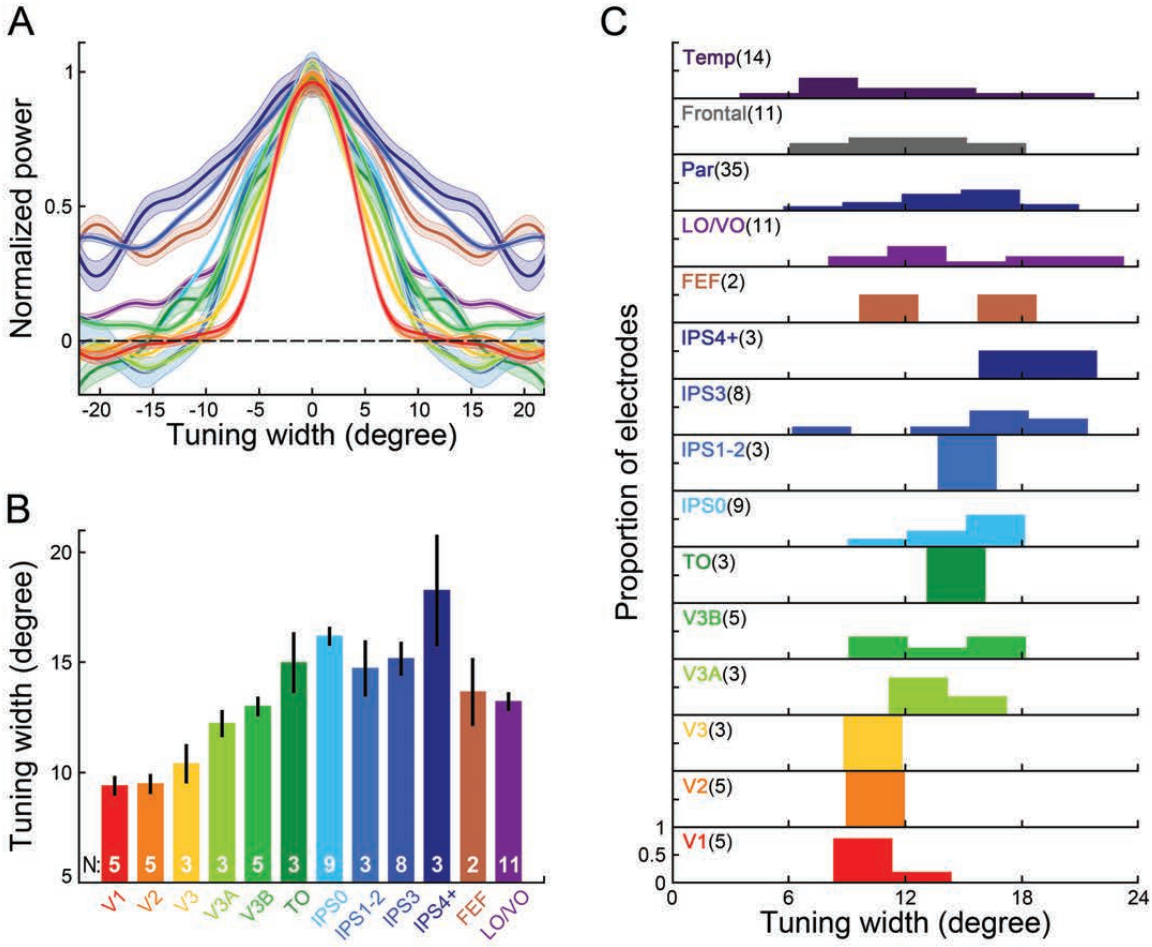

Figure 10

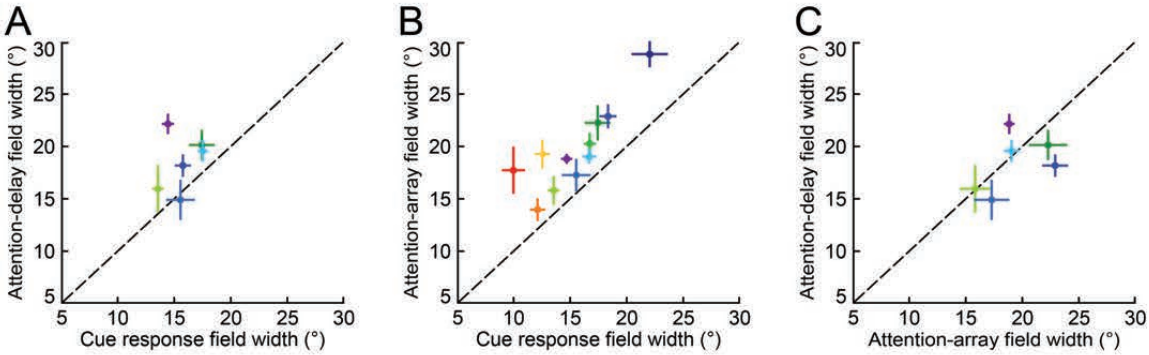

Figure 11